A Stochastic Inversion Method for Potential Field Data: Ant Colony Optimization

Article *in* Pure and Applied Geophysics · October 2013

DOI: 10.1007/s00024-013-0712-8

3 authors, including:

Shuang Liu
China University of Geosciences
46 PUBLICATIONS **311** CITATIONS

SEE PROFILE

Xiangyun Hu
China University of Geosciences，Wuhan，China
129 PUBLICATIONS **1,903** CITATIONS

SEE PROFILE

Pure Appl. Geophys. 171 (2014), 1531–1555

DOI 10.1007/s00024-013-0712-8

Pure and Applied Geophysics

A Stochastic Inversion Method for Potential Field Data: Ant Colony Optimization

Shuang Liu,[1] Xiangyun Hu,[1] and Tianyou Liu[1]

Abstract—Simulating natural ants' foraging behavior, the ant colony optimization (ACO) algorithm performs excellently in combinational optimization problems, for example the traveling salesman problem and the quadratic assignment problem. However, the ACO is seldom used to inverted for gravitational and magnetic data. On the basis of the continuous and multi-dimensional objective function for potential field data optimization inversion, we present the node partition strategy ACO (NP-ACO) algorithm for inversion of model variables of fixed shape and recovery of physical property distributions of complicated shape models. We divide the continuous variables into discrete nodes and ants directionally tour the nodes by use of transition probabilities. We update the pheromone trails by use of Gaussian mapping between the objective function value and the quantity of pheromone. It can analyze the search results in real time and promote the rate of convergence and precision of inversion. Traditional mapping, including the ant-cycle system, weaken the differences between ant individuals and lead to premature convergence. We tested our method by use of synthetic data and real data from scenarios involving gravity and magnetic anomalies. The inverted model variables and recovered physical property distributions were in good agreement with the true values. The ACO algorithm for binary representation imaging and full imaging can recover sharper physical property distributions than traditional linear inversion methods. The ACO has good optimization capability and some excellent characteristics, for example robustness, parallel implementation, and portability, compared with other stochastic metaheuristics.

Key words: Ant colony optimization, potential field data, traveling salesman problem, pheromone, inversion.

1. Introduction

Natural ants are social insects; their individual behavior is simple but their gregarious behavior is quite complex. Swarms of ants working cooperatively can find the shortest path from the nest to a food source (Goss *et al.* 1989; Beckers *et al.* 1992). Biological studies reveal that ant colony members exchange messages with each, mainly by use of chemicals—pheromones—which the ants deposit on their routes. When ants travel they probabilistically tend to choose a route that corresponds to a richer pheromone trail. At the same time the pheromones keep evaporating. So the lengths of routes and the number of ants affect the residual quantities of pheromones. The shorter the routes traveled, the larger the amounts of pheromone deposited. Eventually, the ant colony will find the shortest route (Colorni *et al.* 1991; Dorigo *et al.* 1991).

Inspired by the behavior of natural ants, Colorni, Dorigo, and Maniezzo first presented the ant colony optimization (ACO) algorithm and used it to solve the famous traveling salesman problem (TSP) of combinational optimization problems (COP) in the 1990s (Colorni *et al.* 1991; Dorigo *et al.* 1991; Dorigo, 1992). Since then many modified ACO algorithms had been proposed and widely used to optimize COP. Dorigo *et al.* (1996), for instance, introduced the elitist strategy ACO, that is, after the ant colony finish a tour, irrespective of normally updating the pheromone trails on each path, they still add extra pheromones to the shortest path the ant colony found during the tour. This strategy enhances feedback signals and promotes the rate of convergence. Dorigo and Gambardella (1997a) also used regional and local pheromone updating approaches which promote global search capacity. To overcome the advantages of precocity and stagnation of traditional ACO, Stutzle and Hoos (1997b) introduced the max–min ant system ACO by setting the range of pheromone quantity. Similarly, to increase the speed of evolution of the ant colony, Di Caro and Dorigo (1998a) presented the adaptive ACO, meaning that they adjusted the pheromone trails adaptively on the

[1] Institute of Geophysics and Geomatics, China University of Geosciences, Wuhan, China. E-mail: laushua@foxmail.com; xyhu@cug.edu.cn; liuty@cug.edu.cn

basis of the solutions found. To exploit the advantages of the different algorithms, ACO were also combined with other nonlinear algorithms, for example genetic algorithms (GA) (Pilat and White 2002; Lee *et al.* 2008), simulated annealing algorithms (SA) (Coleman *et al.* 2004), and artificial neural networks (ANN) (Sivagaminathan and Ramakrishnan 2007; Socha and Blum 2007). ACO are currently widely applied to many types of COP, for example the TSP (Dorigo *et al.* 1991, 1996; Gambardella and Dorigo 1995, 1996; Dorigo and Gambardella 1997a, b), the quadratic assignment problem (QAP) (Gambardella *et al.* 1997, 1999b; Stutzle and Hoos 1997a, b, 1998; Maniezzo 1999; Maniezzo and Colorni 1999), the job-shop scheduling problem (JSP) (Colorni *et al.* 1994), the vehicle routing problem (VRP) (Bullnheimer *et al.* 1997, 1999; Gambardella *et al.* 1999a), connection-oriented network routing (Schoonderwoerd *et al.* 1997), and connectionless network routing (Di Caro and Dorigo 1998a, b).

Optimization of the COP is different from geophysical data optimization inversion. The solution space of COP is discrete, and much smaller than that of optimization of the continuous and multi-dimensional objective function of geophysical data. This is the reason ACO are not widely used to invert geophysical data. There are only a few application studies in geophysics. For instance, Chen *et al.* (2005a, b) used ACO to invert the impedances of seismic records of the horizontal layer model. Yan *et al.* (2009) conducted AVO inversion of ACO. Yuan *et al.* (2009) inverted geophysical data using swarm intelligence optimization of the ACO and particle swarm optimization (PSO). Their tests show that the ACO algorithm has many advantages including parallel computation, initial model independence, high robustness, easy constraint, high convergence, and high accuracy (Yuan *et al.* 2009).

To promote the rate of convergence, we modified the traditional ACO algorithm. We present the node partition strategy ACO (NP-ACO) and use it to invert the variables of a specific model and the distributions of physical properties. Concerning the structure, we begin with the methods and theories of potential field data optimization inversion and the artificial ants of the ACO. Subsequently, we discuss the NP-ACO and Gaussian mapping in detail. We also discuss several important variables settings of the NP-ACO and list its advantages and drawbacks compared with other stochastic metaheuristics. The method is then tested by use of synthetic data and by use of real data of gravity and magnetic anomalies. Finally, the paper concludes with a brief discussion.

2. Methods and Theories

2.1. Objective Function for Potential Field Data Inversion

The objective function optimizing potential field data is composed of data constraints and model constraints (Li and Oldenburg 1996, 1998), which is written as:

$$\phi = \phi_{\mathrm{d}} + \lambda \phi_{\mathrm{m}}, \tag{1}$$

where ϕ is the objective function, ϕ_{d} and ϕ_{m} are the data constraints and model constraints, respectively, and λ is the regularization factor to balance the weights between data constraints and model constraints. Usually the weighted l_2-norm of the misfit between observed data and predicted data is defined as the data constraints, namely:

$$\phi_{\mathrm{d}} = \left\| \mathbf{W}_{\mathrm{d}} (\mathbf{d} - \mathbf{d}^{\mathrm{obs}}) \right\|_2^2, \tag{2}$$

where $\mathbf{d}$ and $\mathbf{d}^{\mathrm{obs}}$ are the m-length predicted data vector and observed data vector, respectively. Here, m is the number of observed data, $\mathbf{W}_{\mathrm{d}} = \frac{1}{\sigma_{\mathrm{d}}}\mathbf{I}$ is the weighted matrix for observed data, where σ_{d} is the standard deviations of the observation data, and $\mathbf{I}$ is the unit matrix. As for the model constraints, it is written as:

$$\phi_m = \left\| \mathbf{W}_m (\mathbf{m} - \mathbf{m}_0) \right\|_2^2, \tag{3}$$

here, $\mathbf{m}$ is the n-length model vector of variables to be solved, $\mathbf{m}_0$ is the n-length target model vector of variables, n is the number of model variables, and $\mathbf{W}_{\mathrm{m}}$ is the weighted matrix for model variables. So, finally, inversion of the potential field data is achieved by optimizing the objective function Eq. 1.

2.2. *Artificial Ants*

The ACO algorithm does not directly simulate the behavior of real ants. Artificial ants are proposed. The characteristics of artificial ants are not totally similar to those of real ants (Dorigo *et al.* 1996). For instance, artificial ants in the TSP have memory so they do not visit places twice. Real ants do not have memory and exchange information totally depending on accumulated pheromone intensity on the routes. Also, artificial ants do not choose the path only on the basis of pheromone trails, but also in accordance with heuristic information, for example the distance to next place, meaning that artificial ants have vision. Finally, the artificial ants in the TSP always live in discretely spatio–temporal environments. We do not consider the time consumed by the artificial ants traveling from one place to another. In the real world ants travel in a continuous spatio–temporal domain.

Figure 1 shows how artificial ants find the shortest route (Dorigo *et al.* 1996). The route distances are DH = BH = 1 and DC = BC = 0.5 (Fig. 1a). We assume 30 ants go from A to B and 30 from E to D in each time unit, and each ant walks at a speed of 1 per time unit, and while walking an ant deposits a pheromone trail of intensity 1. At $t = 0$, there is no trail; the 30 ants in B and the 30 in D choose routes with equal probability, therefore 15 ants from each node will go to H and 15 to C (Fig. 1b). After 1 time unit, because the distances B–H–D = 2 and B–C–D = 1, the pheromone intensity on B–H–D is 15, that on B–C–D is 30. Therefore, when another 30 ants traveling from A to B and from E to D choose the routes, on average, 20 ants tend to choose C and 10 ants tend to choose H. So more and more ants tend to choose the shorter route B–C–D (Fig. 1c). This process continues until all the ants eventually choose the shortest path B–C–D.

2.3. *Optimization of Continuous and Multi-Dimensional Function*

The ant colony optimization (ACO) algorithm is primarily used to solve the COP. A typical example is the TSP, that is, how a traveling salesman finds the shortest or least expensive route when he visits each city once. As for potential field data inversion, optimization of the multi-dimensional continuous objective function Eq. 1 is required. Comparison of potential field data optimization inversion and TSP optimization is shown in Table 1. The optimized solution of the objective function is the shortest route in the TSP and the nodes indicate the cities.

When the ACO is used to optimize the continuous function of Eq. 1, first, we divide the continuous model space into discrete nodes. During the constrained ranges $m_i^{\min} \le m_i \le m_i^{\max}$, m_i $(i = 1, 2, \ldots, n)$ is partitioned into N nodes, thereby there are $n \times N$ nodes in total. Here, n is the length of model variable vector, m_i is the ith model variable and $m_i^{\min}$, $m_i^{\max}$ are its minimum and maximum, respectively. We deem model variable m_i as a layer, summing to n layers (Fig. 2a). Starting from the first layer $m_i(i = 1)$, all N_a artificial ants, which randomly locate at the N nodes of the first layer $m_i(i = 1)$, stochastically tour

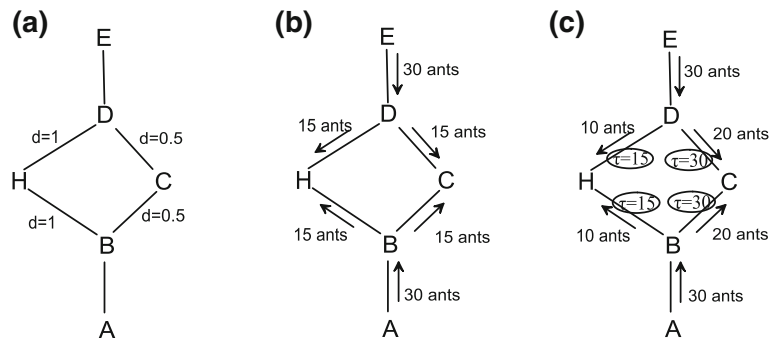

Figure 1
Diagram of ant colony finding the shortest route: **a** the route distances, **b** when $t = 0$ there is no pheromone on the routes and the ants choose routes B–H–D and B–C–D with equal probability, **c** when $t = 1$, the pheromone intensity on route B–C–D is greater than on route B–H–D and more ants tend to choose the route B–C–D

from node $(i-1, j)$ of the $(i-1)$ layer to node (i, k) of the i layer on the basis of transition probability, which is defined as:

$$P_{(i-1,j)}^{(i,k)}(t) = \frac{\left[\tau_{(i,k)}(t)\right]^{\alpha}\left[\eta_{(i,k)}(t)\right]^{\beta}}{\sum_{l=1}^{N}\left[\tau_{(i,l)}(t)\right]^{\alpha}\left[\eta_{(i,l)}(t)\right]^{\beta}}, \quad (4)$$

where $i = 1, 2, \ldots, n-1, j, k = 1, 2, \ldots, N$, $\tau_{(i,k)}$ is the quantity of pheromone at node (i, k), $\eta_{(i,k)}$ is the heuristic function related to some previous information, and α and β are the relatively weighted coefficients of the pheromone trail and heuristic function. Ants keep moving layer-by-layer until they arrive at the last layer m_n. Therefore, every route is a solution. It is assumed that the route toured by the sth ant is solution $\mathbf{m}_s$, corresponding to objective function value ϕ_s. When all ants have completed their tour, the amount of pheromone at node (i, j) is updated on the basis of:

$$\tau_{(i,j)}(t+1) = (1-\rho)\tau_{(i,j)}(t) + \nabla\tau_{(i,j)}(t), \quad (5)$$

where $0 < \rho < 1$, ρ is the volatility coefficient of pheromone trails. The pheromone trails vaporize in the process of the search, which avoids infinite accumulation of pheromone trails and means the ant colony forgets previous long routes. $\nabla\tau_{(i,j)}(t)$ is accumulated pheromone at node (i, j) for all ants. Hence:

$$\nabla\tau_{(i,j)}(t) = \sum_{s=1}^{N_a}\nabla\tau_{(i,j)}^{s}(t), \quad (6)$$

where $\nabla\tau_{(i,j)}^{s}(t)$ is the intensity of pheromone at node (i, j) deposited by the sth ant and N_a is the number of ants.

$\nabla\tau_{(i,j)}^{s}(t)$ is calculated from the objective function for the sth ant and is related to the convergence rate and optimization capability. So, constructing the mapping between the quantity of pheromone on the trails and the objective function values is critical. Dorigo (1992) proposed three ant systems called ant-cycle, ant-density, and ant-quantity, which are widely

Table 1

Comparison between potential field data optimization inversion and the TSP using the ACO algorithm

Optimization for potential field data	Optimization for TSP
Values of objective function	Lengths of routes
Optimum solution	The shortest route
All solutions	All routes
Nodes	Cities

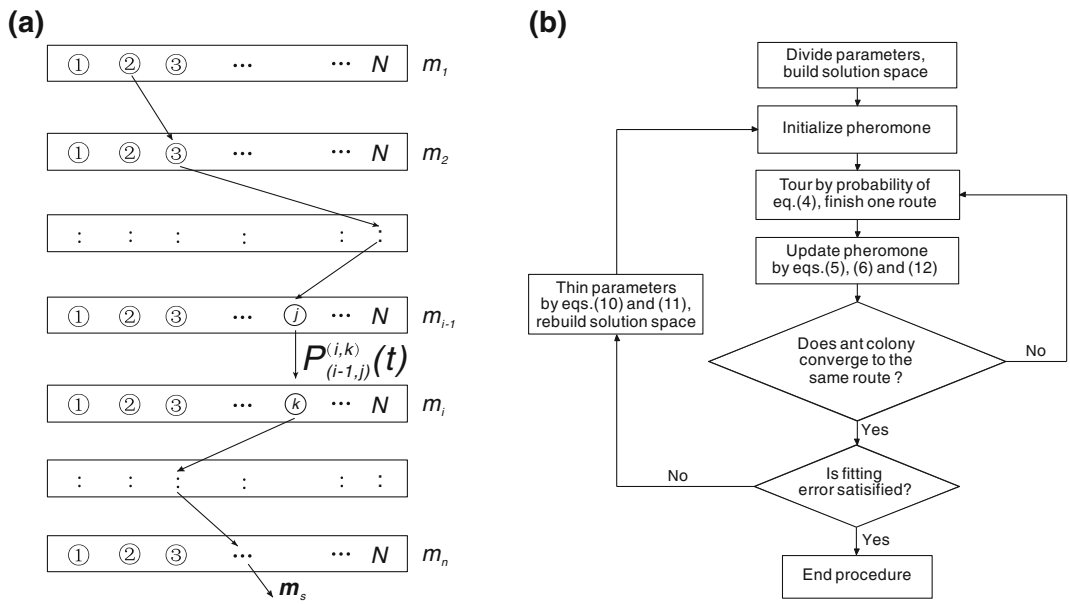

Figure 2

Diagram (**a**) and flowchart (**b**) of NP-ACO optimization of continuous and multi-dimensional functions. m_i (i = 1, 2,…, n) and (i = 1, 2,…, N) are deemed as a layer and a node. Members of the ant colony tour the nodes from the first layer to last layer with transition probability P

used to optimize COP. The definitions of the three ant systems are:

1. Ant-Cycle System

$$\nabla\tau^{s}_{(i,j)}(t) = \begin{cases} \frac{Q}{L_k} & \text{if ant } s \text{ travels the node } (i,j) \\ 0 & \text{otherwise} \end{cases}, \tag{7}$$

where Q is the total amount of pheromone and L_k is the total distance traveled by the kth ant. Hence, if the route is longer, less pheromone will be left on the route. Ants do not leave any pheromone on routes they have not traveled.

2. Ant-Quantity System

$$\nabla\tau^{s}_{(i,j)}(t) = \begin{cases} \frac{Q}{d_{i,j}} & \text{if ant } s \text{ travels the node } (i,j) \\ 0 & \text{otherwise} \end{cases}, \tag{8}$$

where $d_{i,\,j}$ is the distance to the next node (i, j), so the ants always tend to travel the next shorter route.

3. Ant-Density System

$$\nabla\tau^{s}_{(i,j)}(t) = \begin{cases} Q & \text{if ant } s \text{ travels the node } (i,j) \\ 0 & \text{otherwise} \end{cases}, \tag{9}$$

where Q is total quantity of pheromone. The quantity of pheromone is not related to the routes.

In the ant-density and ant-quantity systems, the pheromone is updated when ants move from a node to an adjacent node, whereas in the ant-cycle, the pheromone is updated after all ants finish the tours. Pheromone quantity is a function of tour quality. The ant-cycle, also called most simple ant system (MSAS), performs better than the other two systems and has become the most popular system in practical application (Dorigo and Stutzle 2003).

If ϕ_s, corresponding to the model variable $\mathbf{m}_s$, is smaller, more pheromone trails will be deposited on the nodes and guide the next search. When the ants in the systems finish a tour and update the pheromone trails, they begin a new tour by moving from the last layer m_n to the first layer m_1 according to transition probability. By repeating searches, the ant colony will become concentrated on the shortest route and achieve the optimum solution $\mathbf{m}^*$.

When the ant colony finds the shortest route $\mathbf{m}^*$, all ants become concentrated on the same path and the optimization process is finished. But if the range of model variables is too large, or the number of nodes is small, low inversion precision will result. Therefore, the ant colony can carry out a new search in a new and narrower range, which is adjacent to the optimum solution $\mathbf{m}^*$. Namely the model variable range is reduced by:

$$\text{Space}_i = [m_i^{\min}, m_i^{\max}] \cap [m_i^* - \delta, m_i^* + \delta], \tag{10}$$

here, Space_i is the new range of the ith element of model variable vector $\mathbf{m}$, $\cap$ is the intersection multiplier, $m_i^{\min}$ and $m_i^{\max}$ are the minimum and maximum values of the ith element of model variable vector $\mathbf{m}$, m_i^* is the ith element of the optimum resolution vector $\mathbf{m}^*$, and δ is defined as:

$$\delta = \kappa\frac{m_i^{\min} - m_i^{\max}}{2}(0<\kappa<1), \tag{11}$$

where κ denotes the rapid coefficient reducing the solution range. Therefore, a new solution range is built on the basis of Eqs. 10 and 11, and is smaller than the last solution range. With the same number of nodes, the ant colony can find a more precise route. The flowchart of the NP-ACO algorithm is shown in Fig. 2b.

2.4. Gaussian Mapping

Although the ant systems of Eqs. 7, 8, and 9 have been successfully used to solve the TSP, QAP, and JSP (Dorigo *et al.* 1991, 1996; Dorigo 1992) they are not suitable for potential field data inversion. The potential field data inversion problem is different from the TSP. The former solution space is obtained by dividing continuous variables whereas the latter is intrinsically discrete and is composed of a series of nodes. Thus, the solution space of the TSP is much smaller than that of the multi-dimensional and continuous function. Finding the optimum solution of the TSP is easier than potential field data optimization. The optimizing capacity of ant systems, for example the ant-cycle system, is not powerful. The systems do not reveal differences between ant individuals or solutions in real-time, so ant systems tend to find a locally optimized solution and the iterations converge too early. Although the number of

ants can be increased or the inversion variables can be changed, it is hard to increase the speed and accuracy of inversion.

After all the ants complete a tour, we statistically analyze the search results of the current tour. We then calculate the pheromone trails on the basis of the results of this statistical analysis. So we present a new mapping of the Gaussian function from objective function values to the quantity of pheromone on the trails, which is written as:

$$\nabla\tau^{s}_{(i,j)}(t) = \begin{cases} A\mathrm{e}^{-\frac{\phi_s-\mu(\phi)}{\sigma(\phi)}} & \text{if ant } s \text{ travels the node } (i,j) \\ 0 & \text{otherwise} \end{cases}, \tag{12}$$

where $\mu(\phi)$ and $\sigma(\phi)$ are the mean and deviation of objective function values, respectively. $\mu(\phi)$ and $\sigma(\phi)$ are responsible for adjusting the amount of pheromone dynamically. For two ants $\mathbf{m}'_s$ and $\mathbf{m}''_s$, whose objective function values are ϕ'_1 and ϕ''_1, the ratio of pheromone trails deposited by $\mathbf{m}'_s$ and $\mathbf{m}''_s$ of Gaussian mapping is equal to

$$\frac{\left[\nabla\tau^{s}_{(i,j)}(t)\right]'}{\left[\nabla\tau^{s}_{(i,j)}(t)\right]''} = \mathrm{e}^{\frac{\varphi''-\varphi'}{\sigma}}. \tag{13}$$

For the ant-cycle system, the difference for ant individuals is:

$$\frac{\left[\nabla\tau^{s}_{(i,j)}(t)\right]'}{\left[\nabla\tau^{s}_{(i,j)}(t)\right]''} = \frac{\varphi''}{\varphi'}. \tag{14}$$

Equation 13 highlights the differences among ant individuals more than Eq. 14.

Figure 3 shows the imaging inversion results of magnetic anomalies using ant-cycle mapping and Gaussian mapping. Their inversion variables are set to be the same (i.e. $\lambda = 1{,}000$, $N_a = 200$, $\rho = 0.7$, and $\beta = 3$). The inversion results reveal that the distribution of magnetic cells using ant-cycle mapping is decentralized and is not in good accordance with the theoretical model. Approximately 40 % of magnetic cells are not in the range of the theoretical rectangular model (Fig. 3a). The inversion results using Gaussian mapping are better than the former. First, the distributions of magnetic cells are compact and >90 % of magnetic cells are in the rectangular model (Fig. 3b). The inversion results coincide with the true model. Figure 4 shows the convergence processes of two different mapping models. They show that the ant system of the Gaussian mapping converges faster than the ant-cycle system. The former iterates 97 times when the relative error of fitting observed magnetic anomalies reaches 2 %. The ant system of the ant-cycle model converges slowly. After 1,000 iterations, the fitting error is 18 %. Overall, Gaussian mapping is superior to the ant-cycle system in terms of inversion results and inversion efficiency.

Figure 5 shows the distributions of objective function values using Gaussian mapping. At the beginning of iteration, the random distribution of ants leads to random distribution of objective function values. As the search progresses the mean and deviation of objective function values decrease

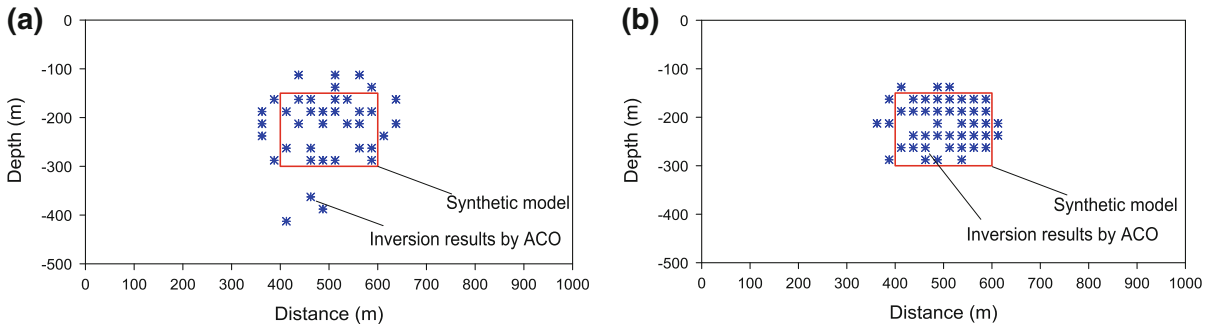

Figure 3
Comparison of inversion results using ant-cycle mapping (**a**) and Gaussian mapping (**b**). Recovered magnetic cell distributions by Gaussian mapping are centralized and highly consistent with the true model whereas the magnetic cell distributions obtained by use of ant-cycle mapping are decentralized. Gaussian mapping yields better inversion results than ant-cycle mapping

gradually which indicates the ant colony is converging. At the last iteration, the objective function values of different ants are the same and finally the ant colony is distribute on the same route.

2.5. *Setting of Variables*

The ant colony optimization (ACO) algorithm has the advantage of strong robustness and its inversion results are not sensitively dependent on the variables used. We now briefly discuss several important variables: regularization factor (λ), priori knowledge of physical properties (susceptibility or density), volatility coefficient (ρ), and numbers of ants (N_a).

1. Regularization Factor (λ)
   The flexibility of choice of the regulation factor (λ) for the ACO algorithm is similar to that for other optimization inversion methods, for example Markov chain Monte Carlo, GA, SA, ANN, etc., and other considerations also are similar. The λ is used to balance the weights between data constraints and model constraints in the objective function. It is critical to choose an appropriate λ to obtain a reasonable inversion result. When λ is too

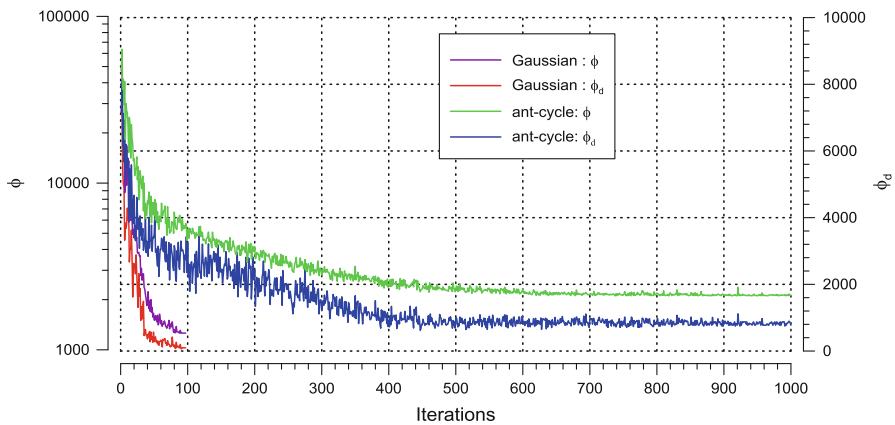

Figure 4
Comparison of convergence processes using ant-cycle mapping and Gaussian mapping. The ant colony converges faster by use of Gaussian mapping than by use of the ant-cycle system

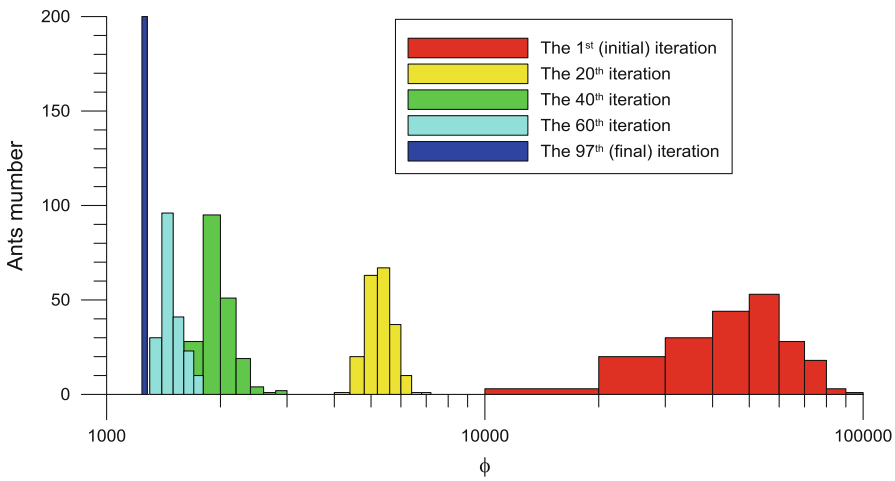

Figure 5
Distributions of objective function values with convergence of the Gaussian mapping NP-ACO. With optimization of the ant colony, the distribution of objective function values decreases and gradually centralizes

small, predicted data are too close a fit to the observed data and the noise in the observed data may distort the inversion results. In contrast, if λ is too large, the predicted data cannot fit the observed data and useful signals are lost. The inverted results tend to be simple.

Three methods are commonly used to determine the λ. The first method is based on the Mozonov's discrepancy principle (Scherzer 1993; Colton *et al.* 1997). If the noise level (φ_d*) in the observed data is known, we change the λ value until $\varphi_d(\lambda) = \varphi_d$*. For this approach we need to know the noise level in the observed data. However, in many practical applications, the noise level is difficult to determine. Under such conditions, another method of determination of λ is generalized cross-validation (GCV) (Golub *et al.* 1979; Golub and Von Matt 1997). The inverted geophysical solutions are stable, so they do not rely on a specific observed datum. Even if this observed datum is not used, the inverted model can predict the specific observed datum. The optimum λ is deemed to be that when the predicted data best fit the observed data. By using the method to choose λ, it is sometimes possible to over-fit the observed data. The GCV also does not have a minimum value. Therefore, these problems make GCV invalid. The third method, which we used in the ACO to determine λ, is based on the Tikhonov curve (Tikhonov and Arsenin 1977), which represents the relationship between data constraints and model constraints in the objective function. The inflection point of the Tikhonov curve is the position of optimum λ. As shown in Fig. 6 from an experiment of imaging inversion of a rectangular model, $\lambda = 700$ is the optimum regularization factor.

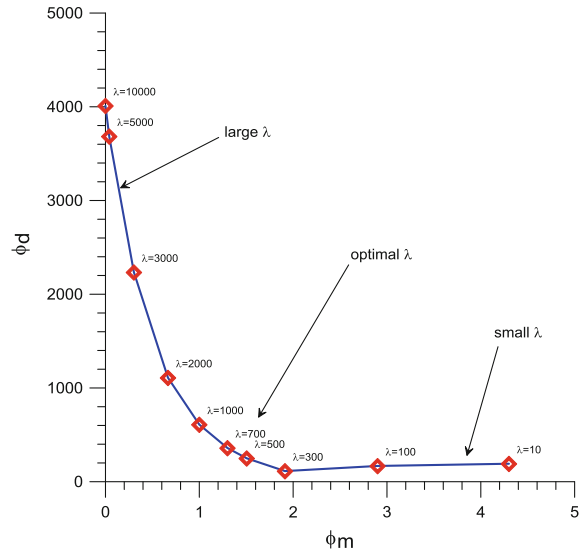

Figure 6
Tikhonov curve: the inflection point of the Tikhonov curve is the position of optimum λ

2. A Priori Knowledge of Physical Properties

When the binary representation ACO is used to perform imaging inversion, it is essential to have the right a priori knowledge of physical properties. The wrong physical properties will lead to unreasonable distributions of physical properties. Figure 7a, b shows the inversion results for incorrect magnetization intensities of 20 and 500 A/m, which are much less and greater, respectively, than the true magnetization intensity of 100 A/m of the rectangular model. Both inverted magnetization distributions are not in accordance with the true rectangular model. The smaller magnetization intensity produces shallower and wider magnetization intensity distributions (Fig. 7a) whereas the larger magnetization intensity yields deeper and narrower magnetization distributions (Fig. 7b). In a real situation, the physical properties can be accurately calculated by measuring the susceptibility and density of ore and rock samples.

3. Volatility Coefficient of Pheromone Trail (ρ)

The volatility coefficient of the pheromone trail (ρ) is important if the ant colony is to find the optimum route. It must avoid too rapid convergence of the algorithm and is implemented as a useful form of forgetting, favoring exploration of new areas in the search space (Socha and Dorigo 2008). When ρ is too small, the solutions which have been searched during the last iterations may be chosen again with larger probability, which decreases random performance and global search ability. In contrast, too large a value of ρ will reduce the rate of convergence. Figure 8a shows the relationship between volatility coefficient and inversion results, and computational efficiency in an inversion test of gravity data. Figure 8a

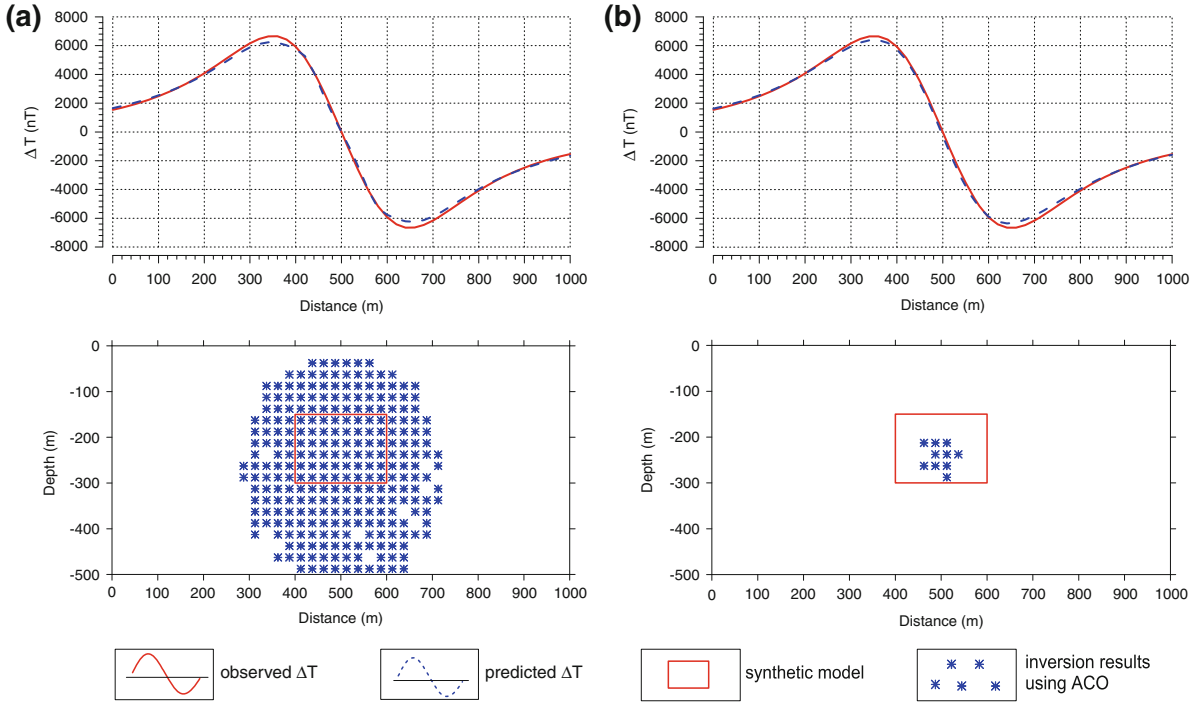

Figure 7
Inversion results from incorrect magnetization intensity setting: **a** $M = 20$ A/m, **b** $M = 500$ A/m. The wrong magnetization intensity damages the inversion results. The larger magnetization intensity produces shallower and wider magnetization intensity distributions whereas the smaller magnetization intensity yields deeper and narrower magnetization distributions. The true magnetization intensity is $M = 100$ A/m

demonstrates that when $0.1 < \rho < 0.8$, predicted data can fit the observed data. With increasing ρ, the calculation time of the NP-ACO algorithm decreases until $\rho = 0.7$, when the time spent is minimum, before computation time tends to increase dramatically. Overall, $0.5 \leq \rho \leq 0.7$ can achieve good search efficiency and a high rate of convergence, which also accords with other published literature, for example Dorigo (1992) and Dorigo *et al.* (1996). In our synthetic and real examples, we set ρ to be a constant (i.e. $\rho = 0.7$).

4. Number of Ants (N_a)
Similar to volatility coefficient, number of ants (N_a) also is an important variable related to global search efficiency and search speed. Dorigo *et al.* (1996) found that the complexity of the ACO algorithm in the TSP is $O(NC \times n^2 \times m)$, where NC is the number of iterations, n is the number of nodes, and m is the number of ants. Also they suggested that the number of ants should be approximately equivalent to the number of nodes. As shown in Fig. 8b of an inversion test of gravity data with different numbers of ants, computation time increases linearly with increasing number of ants whereas fitting error declined with increase of N_a. This demonstrates that many more ant individuals can improve the inversion results but enhance the computational burden. So it is necessary to choose an appropriate N_a to balance inversion precision and computational cost. We suggest that the number of ants is approximately equal to the number of nodes.

2.6. Algorithm Convergence

Convergence analysis of the ACO algorithm is important. Stutzle and Dorigo (2002) proved some convergence properties for a class of ant colony optimization algorithms. They proved that after a sufficiently large number of iterations there is a sufficiently large probability (i.e. tending to 1) of finding an optimum route. They also proved that,

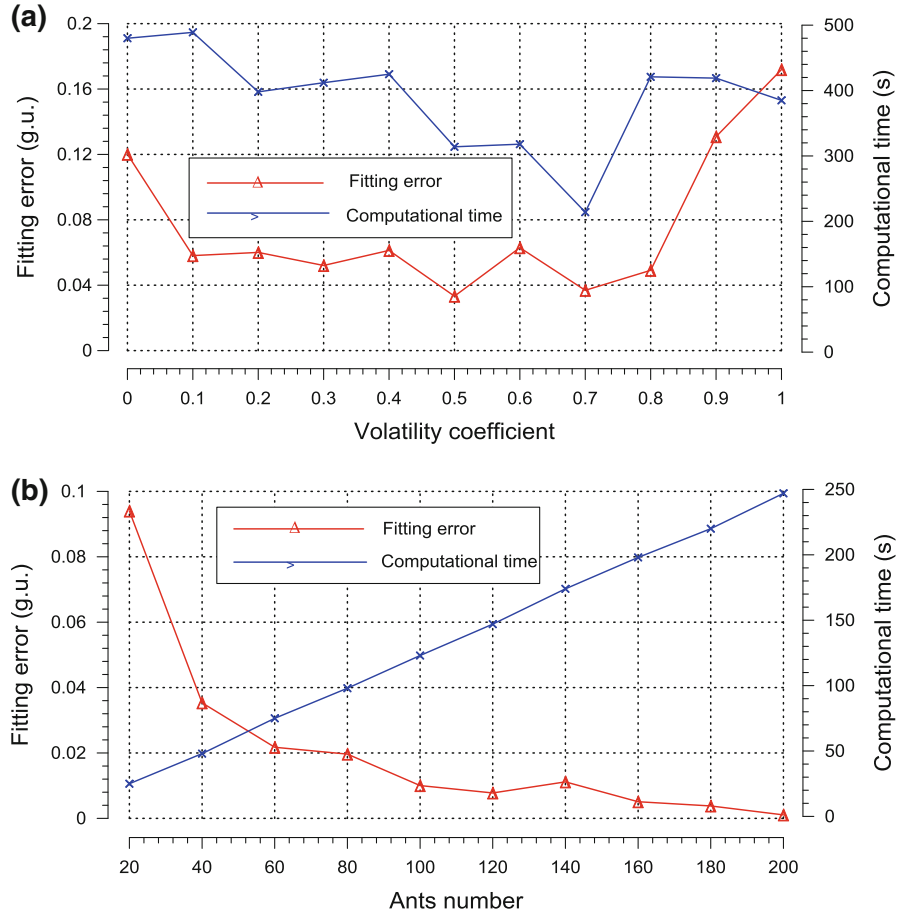

Figure 8
Effects of volatility coefficient (**a**) and number of ants (**b**) on fitting *error* and computation time. Smaller or larger volatility coefficients increase the fitting *error* and computation time. The most appropriate volatility coefficient is $0.5 \leq \rho \leq 0.7$. The computation time increases linearly with the number of ants but can reduce the fitting *error*

after an optimum solution had been found, it takes a finite number of iterations for the pheromone trails associated to the found optimum solution to grow higher than for any other pheromone trail. We now briefly discuss convergence of the ACO algorithm.

It is assumed that the initial quantity of pheromone and the number of ants are τ_0 and N_a, respectively, and the upper limit and lower limit of pheromone quantity that every ant deposits are $\Delta\tau_{max}$ and $\Delta\tau_{min}$, respectively. After t searches, the total quantity of pheromone is:

$$\tau(t) \leq \tau_{max}(t) = (1-\rho)^t \tau_0 + N_a \Delta\tau_{max} \frac{1-(1-\rho)^t}{\rho} \quad (0 < \rho < 1). \tag{15}$$

Hence, calculating the limit of Eq. 15 furnishes:

$$\lim_{t\to\infty} \tau(t) \leq \lim_{t\to\infty} \tau_{max}(t) = \frac{N_a \Delta\tau_{max}}{\rho} = \frac{\Gamma_{max}}{\rho}, \tag{16}$$

which indicates that the quantity of pheromone at each node will eventually reach a constant level and the search process will converge after sufficient search time. It is impossible for the total quantity of pheromone at each node to reach infinity, leading to breakdown of the ants system. If ants system searches for a sufficient time, the pheromone will arrive at a saturated state, which is directly proportional to the number of ants N_a and the maximum increment of pheromone $\Delta\tau_{max}$ and inversely proportional to volatility ρ, but not related to the initial state.

2.7. Algorithm Characteristics

The ACO in essence belongs to the well-known stochastic metaheuristics, for example Monte Carlo (MC), neural networks (NN), and evolutionary computation (EC). The ACO has many similarities with these approaches (Dorigo *et al.* 1999). For example, the ACO can be interpreted as a parallel replicated Monte Carlo system. Monte Carlo systems are general stochastic simulation systems, that is, techniques performing repeated sampling experiments on the model of the system under consideration by making use of a stochastic component in the state sampling and transition rules (Dorigo *et al.* 1999). Also, ant colonies, being composed of numerous concurrently and locally interacting units, can be seen as "connectionist" systems, the most famous examples of which are neural networks. Structurally, the parallel between the ACO metaheuristic and a generic neural network is obtained by putting each state visited by ants as equivalent to a neuron, and the problem-specific neighborhood structure of a state as equivalent to the set of synaptic-like links exiting the neuron. The ants themselves can be seen as input signals concurrently propagating through the neural network and modifying the strength of the synaptic-like interneuron connections (Dorigo *et al.* 1999). There are also general similarities between the ACO metaheuristic and the EC. Both approaches use a population of individuals that represent problem solutions, and in both approaches knowledge about the problem collected by the population is used to generate stochastically a new population of individuals. A major difference is that in EC algorithms all the knowledge about the problem is contained in the current population, whereas in the ACO a memory of past performance is maintained in the form of pheromone trails (Dorigo *et al.* 1999).

Compared with other stochastic metaheuristics, the ACO has the advantages of good optimization ability and steady convergence. The ACO is capable of finding the shortest path by relying directly on the intensity of the pheromone trail at the nodes deposited by the ants. This is a positive feedback (autocatalytic) mechanism (Dorigo and Gambardella 1997b), which makes ant systems eventually converge to the same routes after a limited number of iterations, as proved in Eqs. 15 and 16. The ACO is also used to optimize the objective function. If we have developed the interface between the objective function and the ant system, the ACO algorithm can be conveniently applied to other optimization problems and the inversion results of the ACO also do not depend on the starting routes. So the ACO is more robust (Dorigo and Gambardella 1997b; Dorigo *et al.* 1999; Socha and Dorigo 2008). Simultaneously, the ACO is a kind of parallel implementation algorithm (Dorigo and Gambardella 1997b; Dorigo *et al.* 1999). Each ant individual's search behavior is independent and they communicate with each other on the basis of pheromone trails on the paths. So the ACO can be regarded as a distributed and multi-agent system. The ant colony begins to search at the same time and also search independently, which increases the reliability of algorithm and also means the algorithm has good global search ability. This parallel function has the advantage of realizing parallel implementation, which can be used to solve some complicated problems. In addition, the ACO is easily combined with other stochastic metaheuristics, for example GA (Pilat and White 2002; Lee *et al.* 2008), SA (Coleman *et al.* 2004), and ANN (Sivagaminathan and Ramakrishnan 2007; Socha and Blum 2007). This characteristic can make full use of the advantages of the different algorithms. Therefore, the ACO has the potential to be a popular approach in geophysical inversion, similar to MC, GA, SA, etc. However, ACO has some drawbacks. For instance, the computation time of the method is usually long. The ACO is also prone to mature too early and discover a local extremum (Dorigo and Blum 2005), although we propose use of the Gaussian ant system to improve computational efficiency.

3. Synthetic Examples

3.1. Variable Inversion

There are two kinds of inversion method for potential field data: variable inversion and imaging inversion. In variable inversion the shapes of the geological models are fixed and we must invert the

geometric and physical properties. For example, a two-dimensional (2D) dyke can be assumed to be a tabular plate. We invert the properties of a tabular plate, including its depth, width, length, inclination, and magnetization intensity, and direction, to describe the geological body. Therefore, variable inversion is, depending on the specific model, more suited to some simple geological situations. Imaging inversion entails recovering the distribution of the physical properties (i.e. density and susceptibility) after division of the subsurface into a number of mesh cells. On the basis of the physical property distributions we can study ores and rocks. Hence, imaging inversion has the capacity to recover complicated distributions of density and susceptibility. Usually, the number of observations is much greater than the dimensions of the model variables, so the objective function of variable inversion does not contain the model constraints, i.e.:

$$\phi_m = 0. \tag{17}$$

We design a three-dimensional (3D) magnetic cuboid model to test the method; the projections in the eastern, northern, and depth directions are shown in Fig. 9a–c. Its central coordinates are $(x_0, y_0, z_0) = (500, 500, 250\ \text{m})$. Extending the lengths in three directions are $(a, b, c) = (100, 200, 100\ \text{m})$. Its magnetization magnitude is $M = 120$ A/m with inclination $I = 45°$ and declination $D = 0°$. The synthetic total field anomaly is shown in Fig. 9a. The line spacing and point spacing of observations are 50 m. There are 21 lines and each line has 21 observation points. The total number of observation points is 441. The solved variable vector is $\mathbf{m} = (M, I, x_0, y_0, z_0, a, b, c)$.

We invert the eight variables (i.e. M, I, x_0, y_0, z_0, a, b, c) of the cuboid on the basis of the synthetic total magnetic anomaly in Fig. 9a. We set the number of ants as $N_a = 500$ and the pheromone volatility coefficient as $\rho = 0.7$. The limited ranges of eight variables are shown in Table 2. Each variable in its limited range is equally divided into 100 nodes. Therefore, there are eight layers, 800 nodes, and 100^8 routes (Fig. 2a). The ant colony will find the shortest path from the 100^8 routes. At the same time, we reduce the solution space by $\kappa = 2/3$. First, we

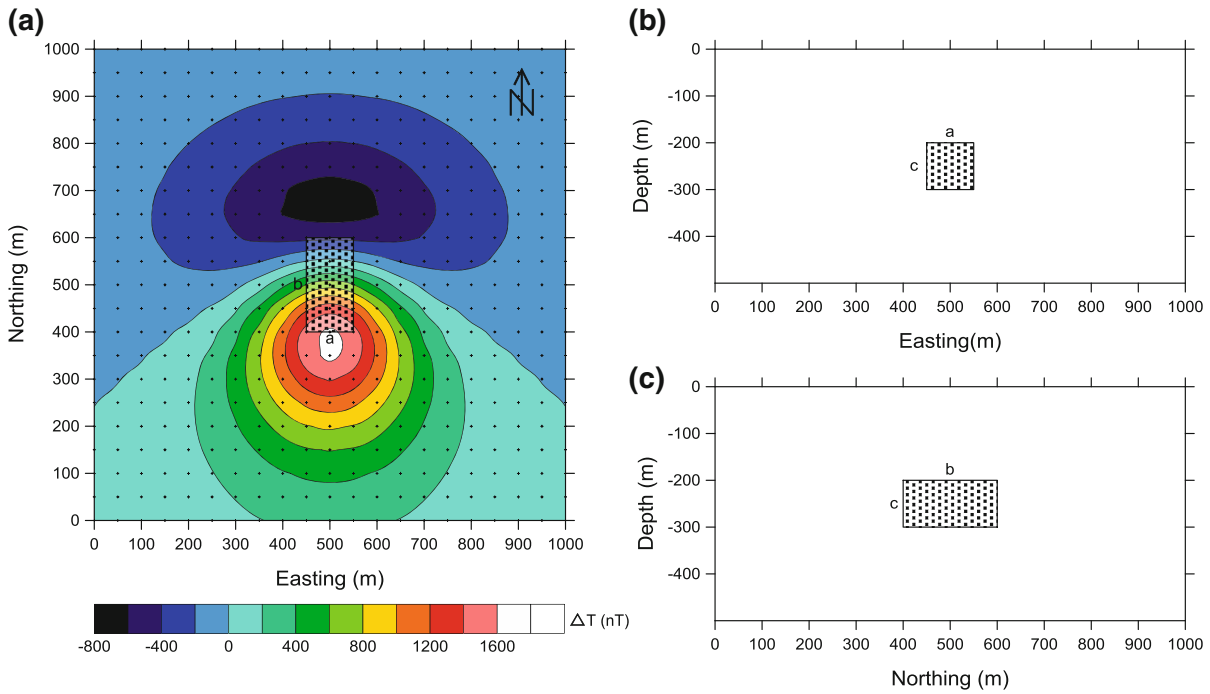

Figure 9
Total field anomaly (ΔT) and projections of the cuboid model at three cross-sections: **a** total field anomaly and horizontal projection, **b** eastern projection, **c** northern projection

Table 2

Variable inversion results for magnetic data of the cuboid model using the NP-ACO

Variables	M (A/m)	I (°)	x_0 (m)	y_0 (m)	z_0 (m)	a (m)	b (m)	c (m)	Iterations	Error (nT)
True values	120	45	500	500	250	100	200	100	–	–
Ranges	0–500	0–180	0–1,000	0–1,000	0–500	0–500	0–500	0–500	–	–
$\alpha = 1, \beta = 0$	135.2	45.3	500.0	498.8	256.7	100.2	173.0	105.0	491	6.9
$\alpha = 0.8, \beta = 0.2$	125.5	45.0	499.9	499.8	251.6	98.4	197.3	99.3	434	1.5

The inverted variables are in agreement with true values and the heuristic information can improve the inversion precision

assume there is no heuristic information (i.e. $\alpha = 1$, $\beta = 0$). The research results for the ant colony are shown in Table 2.

The ACO has strong search ability and the rate of convergence is steady. After 491 iterations the ant colony converges to the optimum route and good approximations to the true values are obtained. For example, the precision of magnetization inclination reaches 0.3° (i.e. 45.3°–45°). The error of the cuboid's horizontal location is <1.2 m (500–498.8 m), and the depth error is 6.7 m (256.7–250 m). The ant colony also successfully inverts the magnetization intensity and lengths of the cuboid except for variable b (the length in the northern direction), for which the error is 27 m. In summary, the ACO achieves a good inversion result.

When $\alpha = 1$ and $\beta = 0$ the ant colony is avaricious, and finds the shortest route entirely by depending on pheromone intensity or objective function value for each route without any heuristic information. If we provide some heuristic information to the ant system, it can guide the tour and reduce the search time. We assume that the lengths of cuboid obey the normal distributions: $a \sim N(100, 50)$, $b \sim N(200, 50)$, $c \sim N(100, 50)$. The distributions of other variables are homogeneous. So the heuristic function $\eta_{i,k} = CP_{i,k}$, where C is a constant and $P_{i,k}$ is probability distribution. We assume $\alpha = 0.8$ and $\beta = 0.2$; the inversion results are listed in Table 2.

As can be seen from Table 2, the ant system with heuristic information converges faster than without any a priori information. Also, the inverted variables, especially the lengths of the cuboid, are better than the inversion results without any heuristic information. The heuristic function can guide the search of the ant system to the optimum path.

3.2. Imaging Inversion

In imaging inversion of potential field data the distributions of the physical properties are recovered by calculating the cells' density or susceptibility after division of the subsurface into mesh cells. Depending on the different partition numbers, we present two kinds of imaging inversion method: binary representation imaging and full imaging. If the geological boundary between two kinds of medium is clear and the physical properties are distributed homogeneously and steadily, the model variables are divided into two nodes, 0 and 1. The 0 represents cells which do not have density or susceptibility contrast whereas the 1 represents cell with density or susceptibility contrast. This binary representation method is an effective means of revealing geophysical non-uniqueness by reducing the solution space. It is suitable for situations in which the target bodies, for example sedimentary iron ores and granite rocks, have obvious and steady contrasts of physical properties. When, on the other hand, susceptibility and density are distributed inhomogeneously and the geological boundary is a transitional type, for example metamorphic iron ores, the distributions of physical properties should be recovered by use of the full imaging approach in which the variables of each model are divided among tens or hundreds of nodes rather than two nodes only. We used the binary representation imaging and full imaging methods to test the ACO algorithm.

In the variable inversion example, the objective function does not contain model constraints because the number of variables is small. In imaging inversion, the subsurface is divided into hundreds of cells, which is greater than the number of observation points. So the inversion problem is under-determined.

Therefore, it is essential to constrain the model to be simple and reasonable. In imaging inversion of the NP-ACO, the model constraint is defined as:

$$\varphi_m = \frac{\left(\sum_i^n |\mathbf{r}_i - \mathbf{r}_0|/n\right)}{(z - z_0)^{\beta/2}}, \tag{18}$$

where the numerator minimizes the model variables and guarantees that the volumes and distributions of anomalous bodies are simple and reasonable, and the denominator is the depth weighting for the cells. Here, $\mathbf{r}_i$ is the displacement vector of the ith anomalous cell and $\mathbf{r}_0$ is the average displacement vector for all the anomalous cells. z is the depth of the cells and z_0 is a constant for depth. β is the depth-weighted coefficient which is related to the rapid attenuation of gravity and to magnetic anomalies with increasing cell depth (Li and Oldenburg 1996, 1998). As for different inversion problems, the choices of β are different. For 2D magnetic imaging, $\beta \leq 4.0$ whereas for 3D magnetic imaging, $\beta \leq 6.0$. For 2D gravitational imaging, $\beta \leq 2.0$ and for 3D gravitational imaging, $\beta \leq 4.0$.

We designed six kinds of 2D magnetic prism models to do the imaging inversion and to test the methods. As shown in Fig. 11a–f, the six synthetic models are the single rectangular prism, the single dipping prism, the combinational parallel prism, the combinational syncline prism, the combinational cut prism, and the combinational reproduction prism. Some of the models or their approximations have appeared in other published literature (Li and Oldenburg 1996, 1998, 2000; Pilkington 1997; Zhang 2003; Liu 2007; Lelievre and Oldenburg 2009), which is benefit for comparison of inversion results. The magnetization intensity $M = 100$ A/m and the magnetization inclination $I = 45°$. The synthetic total field anomalies (ΔT) are also shown in Fig. 10a–f (red lines). The point spacing is 20 m and the number of observation points is 51. Because the prisms are magnetized with inclined magnetization (i.e. 45°), the total field anomalies are concomitant with positive and negative values (Fig. 10a–f).

When we recover the magnetization distributions by use of the binary representation imaging and full imaging methods, the variables are set as in Table 3. The variables of the six models, including N_a, ρ, and β, are set to the same values except for the regularization factor (λ). The number of ants (N_a) is 500, the volatility coefficient (ρ) is 0.7, and the depth weighted index (β) is 3.0. The regularization factors of the six prism models are determined by use of the Tikhonov curve (Fig. 6), the reflection point of which represents the optimum regularization factor. The regularization factors (λ) of the six prism models are varied from 300 to 800 (Table 3). In addition, the subsurface of the six models is divided into 20 rows × 40 columns = 800 rectangular cells whose size is 25 m × 25 m. As for binary representation imaging inversion, each cell's physical property is partitioned into two nodes, denoted 0 and 1. As mentioned above, 0 represents cells with no magnetic contrast whereas 1 represents cells with magnetic contrast of 100 A/m. Thus, there are 800 layers, 1,600 nodes, and 2^{800} routes, in total, in Fig. 2a. The ant colony will find the optimum path from the 2^{800} routes. For full imaging inversion, the magnetization intensity is equally divided into 20 nodes in the range 0–100 A/m. Hence, in total, there are 800 layers, 16,000 nodes, and 20^{800} routes. The ant colony will find the optimum path from the 20^{800} routes (Fig. 2a). Therefore, irrespective of whether the binary representation imaging method or full imaging method is used, the potential data inversion is a difficult optimization problem that finds the optimum path from the large number of routes.

Figures 11 and 12 show the imaging inversion results from the six prism models using binary representation imaging and full imaging inversion, respectively. Both binary representation imaging and full imaging achieve perfect inversion results. First, the ACO has good optimization capacity and stable convergence is achieved. As can been seen from Table 3, after a few hundred iterations the ant colony converges on the same route. The data predicted by binary representation imaging and full imaging accurately fit the observed data, as shown in Fig. 10. Second, with regard to the inversion results, the recovered magnetization distributions for the single rectangular and dipping prism, including their buried depths, horizontal locations, widths, lengths, and dipping angles are in good agreement with the true models (Figs. 11a, b, 12a, b). For other combinational models, there are some discrepancies between the recovered magnetization distributions

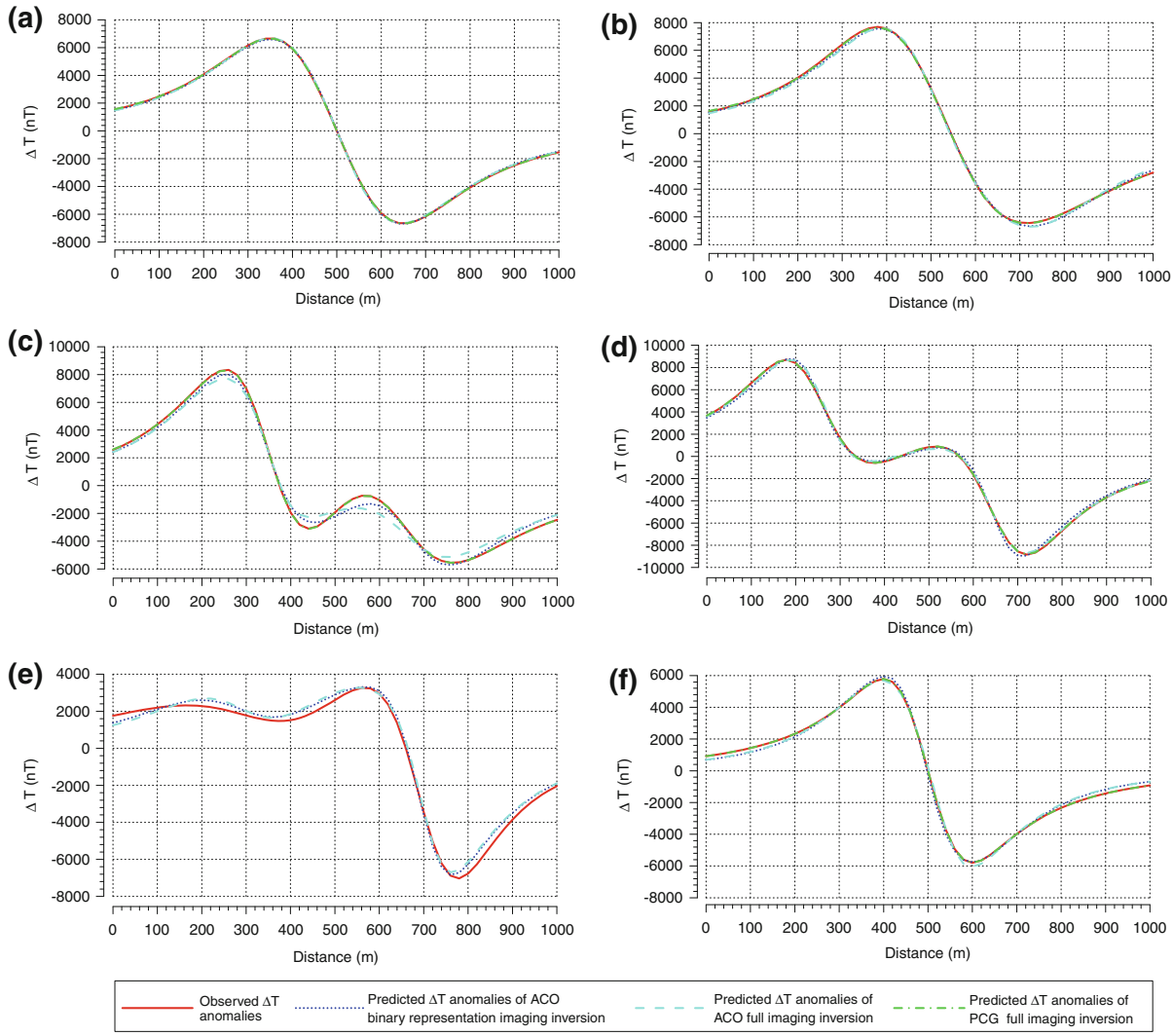

Figure 10

Observed and predicted ΔT anomalies of the ACO binary representation imaging inversion, the ACO full imaging inversion, and the PCG full imaging inversion of the six synthetic prism models: **a** rectangular prism, **b** dipping prism, **c** parallel prism, **d** syncline prism, **e** cut prism, **f** reproduction prism. All terms of the predicted data accurately fit the observed magnetic anomalies

and the true models, but the primary characteristics coincide with the theoretical models. Because the ground potential field data have low resolution in the vertical direction, it is difficult to entirely distinguish the closed two prisms of the syncline model in Figs. 11d, and 12d, and the two parallel prisms of Figs. 11c, and 12c tend to be connected. The similar model of parallel prisms of Figs. 11c, and 12c, was tested by Li and Oldenburg (2000). Their imaging results also revealed that if ground magnetic data, only, is used the two magnetic bodies cannot be totally distinguished. Hence, they combined surface magnetic data with three-component borehole magnetic data to improve the inversion quality. When Li and Oldenburg (1998), Zhang (2003), and Liu (2007) recovered the density distributions of gravity data, they also mentioned the syncline model of Figs. 11d and 12d. In their tests, two wings of the syncline model also cannot be clearly distinguished. In addition, because of serious suppression by shallow resources' strong anomalies of weak anomalies of deep resources, the ACO algorithm does not

Table 3

Variables used in the ACO binary representation imaging and the full imaging of the six prism models

Imaging type	Figure	Model	Partitions	λ	N_a	ρ	β	Iterations
Binary representation imaging	11a	Rectangular prism	2	800	500	0.7	3.0	141
	11b	Dipping prism	2	500	500	0.7	3.0	208
	11c	Parallel prism	2	600	500	0.7	3.0	166
	11d	Syncline prism	2	300	500	0.7	3.0	260
	11e	Cut prism	2	300	500	0.7	3.0	196
	11f	Reproduction prism	2	600	500	0.7	3.0	112
Full imaging	12a	Rectangular prism	20	800	500	0.7	3.0	131
	12b	Dipping prism	20	700	500	0.7	3.0	135
	12c	Parallel prism	20	500	500	0.7	3.0	130
	12d	Syncline prism	20	300	500	0.7	3.0	188
	12e	Cut prism	20	600	500	0.7	3.0	183
	12f	Reproduction prism	20	600	500	0.7	3.0	124

model the deeper prisms, for example the cut and reproduction prisms in Figs. 11e, f, and 12e, f, as well as combinational models. Similar behavior has been reported by Li and Oldenburg (1996), Zhang (2003), and Liu (2007).

We also performed imaging inversion for the six prism models by using the preconditioned conjugate gradient (PCG) method (Pilkington 1997). PCG yields a good approximation of the true models. However, the recovered magnetization intensity tends to distribute smoothly (Fig. 13). For example, the ranges of magnetization intensity distributions are always larger than the regions of the true models and the recovered maximum intensity of magnetization is only approximately 60 A/m, which is far less than the true magnetization intensity (i.e. 100 A/m). The magnetization intensity distributions are so smooth it is difficult to determine the physical property boundary from the images of magnetization distributions of Fig. 13, whereas both ACO binary representation imaging and full imaging produce sharp magnetization distributions, as shown in Figs. 11 and 12. The magnetization intensity of all magnetic cells of binary representation imaging is 100 A/m. In full imaging, the inverted magnetization intensity varies from 75 to 100 A/m, which is in accordance with the true magnetization intensity (i.e. 100 A/m). Therefore, compared with linear inversion approaches, for example PCG, the binary representation imaging and full imaging ACO algorithm have the advantage of recovering the physical property distributions with sharp boundaries whereas traditional inversion methods produce smooth physical property distributions of lower resolution.

In summary, the tests on the six synthetic prism models furnished favorable inversion results. The ACO has the merits of good optimization ability, steady convergence rate, and being capable of producing sharp physical property distributions.

4. *Prospecting for Magnetite Using Magnetic Data in Galinge Deposit, Qinghai, Northwestern China*

4.1. *Geology and Geophysics*

The Galinge iron-ore deposit is located in the Qimantage chasmic trough in the East Kunlun orogenic belt, Qinghai province, Northwestern China (Qi *et al.* 2010; Zhang *et al.* 2011). In this region, the basic rock is not outcropped but is covered by wide and thick Quaternary gravels (Q) of thickness 117–210 m. The defined stratum sequence, syngenetic breccia of the horizons, and volcanic and subvolcanic rocks in the area are the major factors determining the form of iron in the deposit. The ore bodies of the deposit are mainly distributed in the Ordovician Tanjianshan group (OST) lithological segment of marble (Fig. 14a). The major wall-rock alterations closely associated with mineralization include skarnization and serpentinization. The ore minerals are mainly magnetite, with smaller amounts of hematite and siderite. The Galinge iron-ore deposit

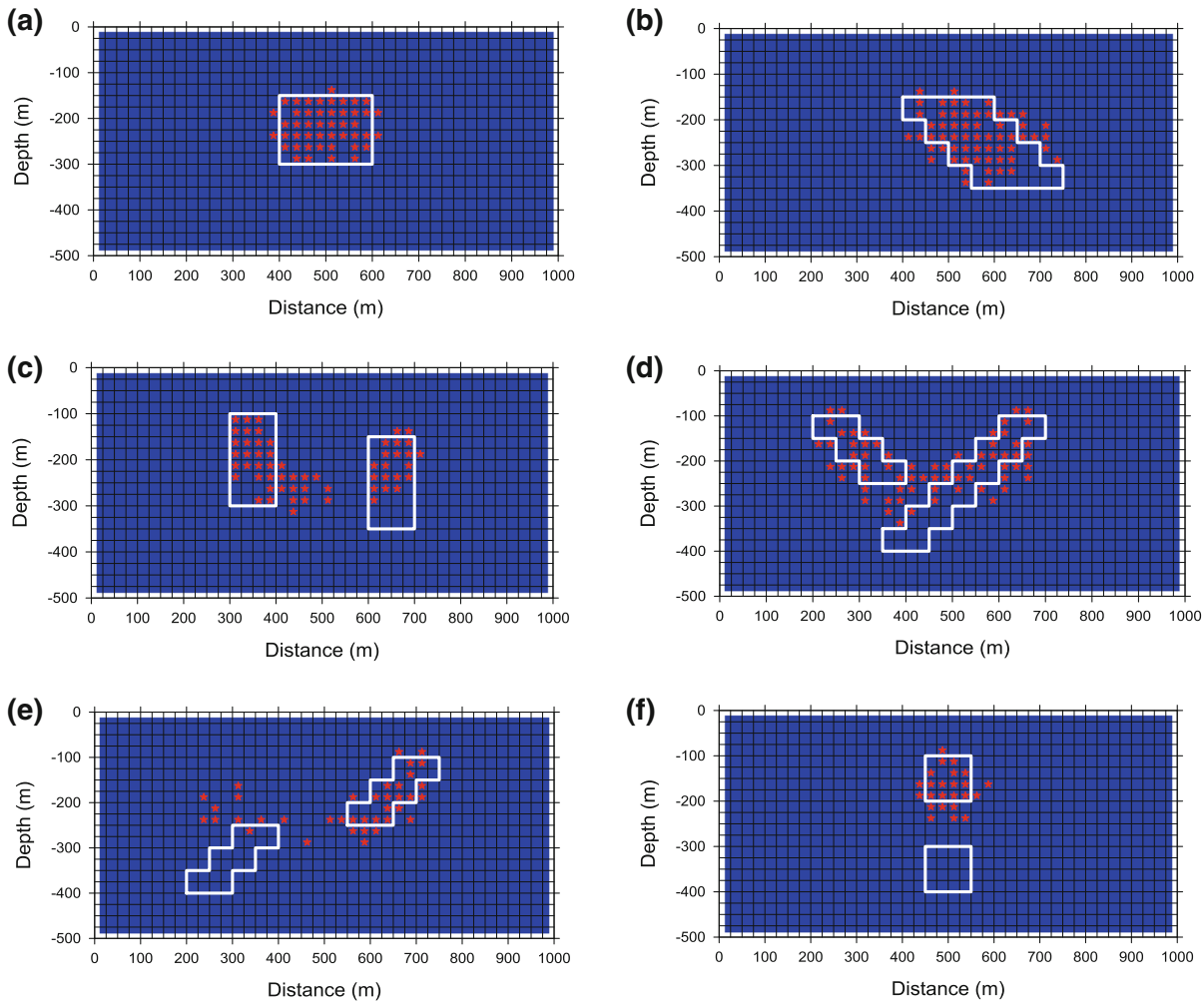

Figure 11
ACO binary representation imaging inversion results for the six synthetic prism models: **a** rectangular prism, **b** dipping prism, **c** parallel prism, **d** syncline prism, **e** cut prism, **f** reproduction prism. The ACO yields a good approximation of the true models and produces sharp magnetization intensity distributions

might have been formed by volcanic exhalation and sedimentation as a reformed and superimposed deposit.

The magnetite bodies in this deposit are totally covered by the wide and thick quaternary gravels. Magnetic prospecting is one of the most effective approaches for locating magnetite deposits. The contour map of total magnetic intensity anomalies reveals there are apparent and regular anomalies whose length and width are $\sim$1,200 and 500 m, which are elliptoid in shape, which lie in the NW–SE direction, and whose amplitude exceeds 1,500 nT (Fig. 14b).

The statistics of magnetic properties of rock and ore samples listed in Table 4 show that the surrounding rocks, for example marble, diorite, and siliceous mud are of low magnetic intensity and include remanent and induced magnetization whereas the dense-massive or sparse-disseminated magnetite is of high magnetic susceptibility. Table 4 also shows that magnetite ores have weak remanent magnetization, and that the ratio of remanent magnetization to induced magnetization of the magnetite samples is 0.22–0.24. Therefore, the magnetite can cause obvious magnetic anomalies and magnetic prospecting is one of the most effective approaches for locating

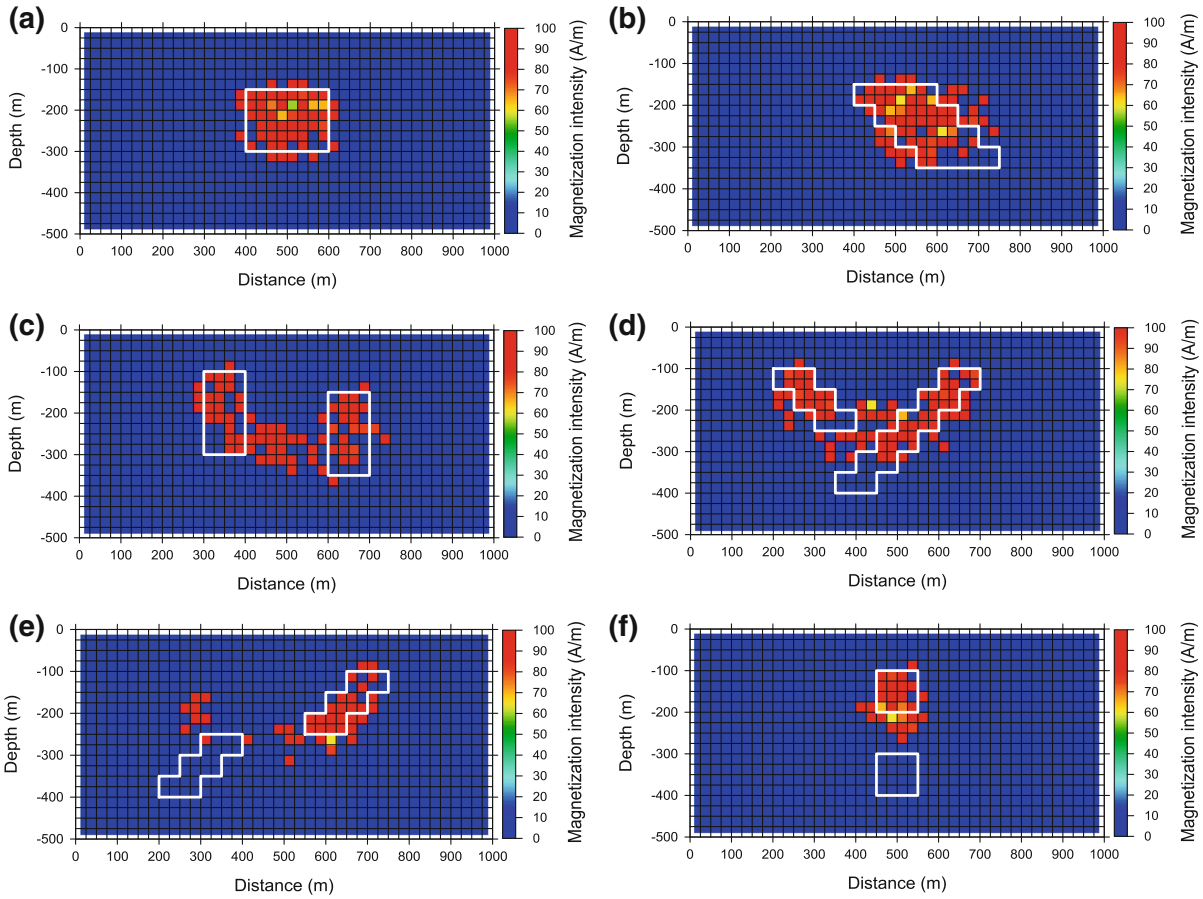

Figure 12
ACO full imaging inversion results for the six synthetic prism models: **a** rectangular prism, **b** dipping prism, **c** parallel prism, **d** syncline prism, **e** cut prism, **f** reproduction prism. The ACO yields a good approximation of the true models and produces sharp magnetization intensity distributions

magnetite ore deposits. Total magnetic field intensity $T_0 = 53{,}800$ nT, geomagnetic inclination $I = 56°$, and geomagnetic declination $I = 356°$ from north to east.

4.2. *Prospecting for Magnetite Along Lines 212 and 196 (Fig. 14a) by Use of NP-ACO*

When we inverted the 2D distributions of magnetite, we assumed the number of ants was 200 and the volatility coefficient was 0.7. Both Line 212 and Line 196 are divided into 40 columns × 20 rows = 800 magnetic cells. According to magnetic properties measurements, the average magnetization intensity is 40 A/m and the magnetization direction lies in the geomagnetic field. In addition, the number of observation points in both Line 212 and Line 196 are 61 and the point spacing is 20 m. We used the binary representation imaging method to recover the distributions of the magnetite ores.

Figures 15 and 16 show the inversion results for Line 212 and Line 196 obtained by use of NP-ACO. After 63 and 112 searches, the ants system converges steadily and the predicted anomalies fit the observed anomalies accurately. Moreover, for Line 212 and Line 196 the magnetite ores inverted by use of the NP-ACO algorithm incline to SW approximately 60°–80°, are located at 2,800 m–3,080 m elevation, and the top-buried depth is approximately 200 m. The inverted magnetite bodies' shapes and occurrence are highly consistent with the presence of magnetite inferred from drillholes (Figs. 15b, 16b).

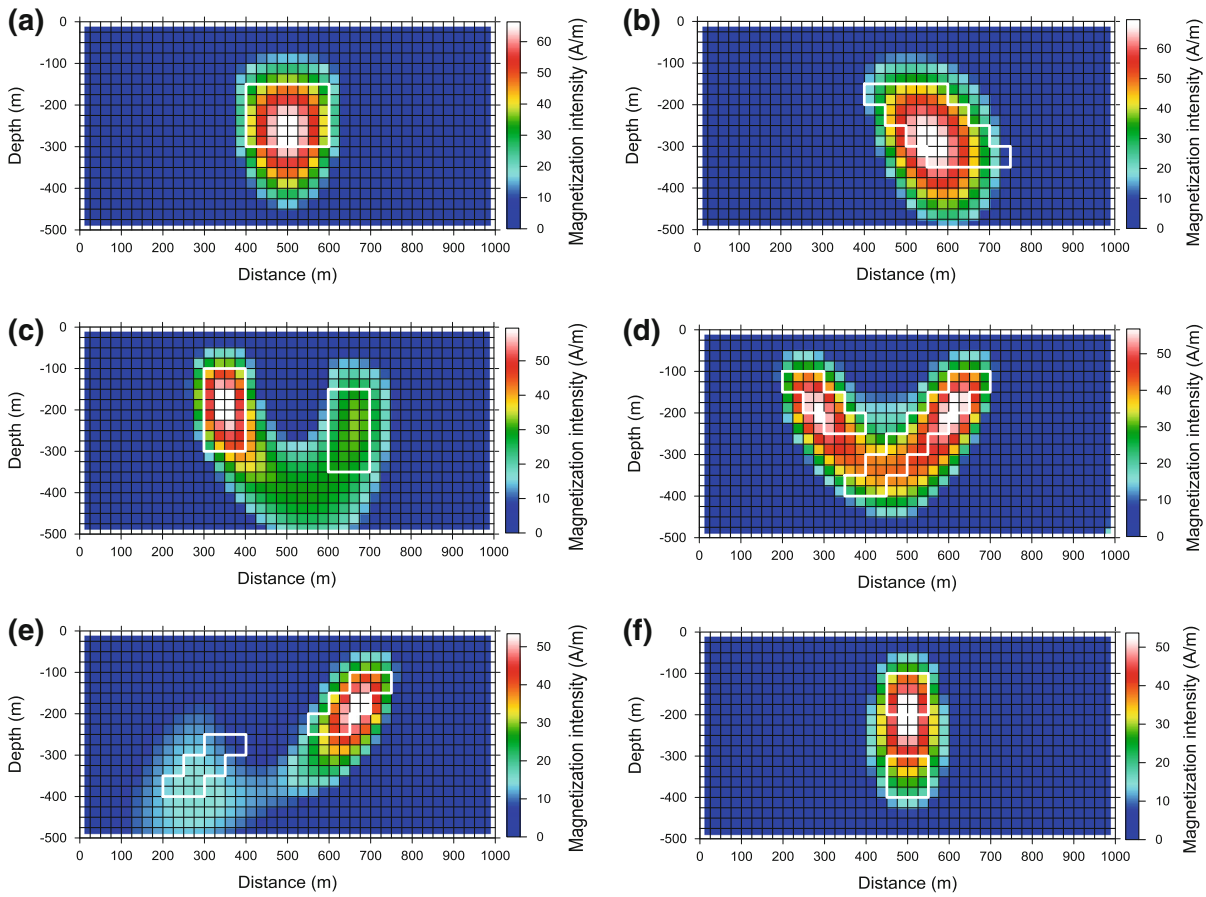

Figure 13
PCG full imaging inversion results for the six synthetic prism models: **a** rectangular prism, **b** dipping prism, **c** parallel prism, **d** syncline prism, **e** cut prism, **f** reproduction prism. The inversion results are consistent with the true models, but PCG produces smooth magnetization intensity distributions

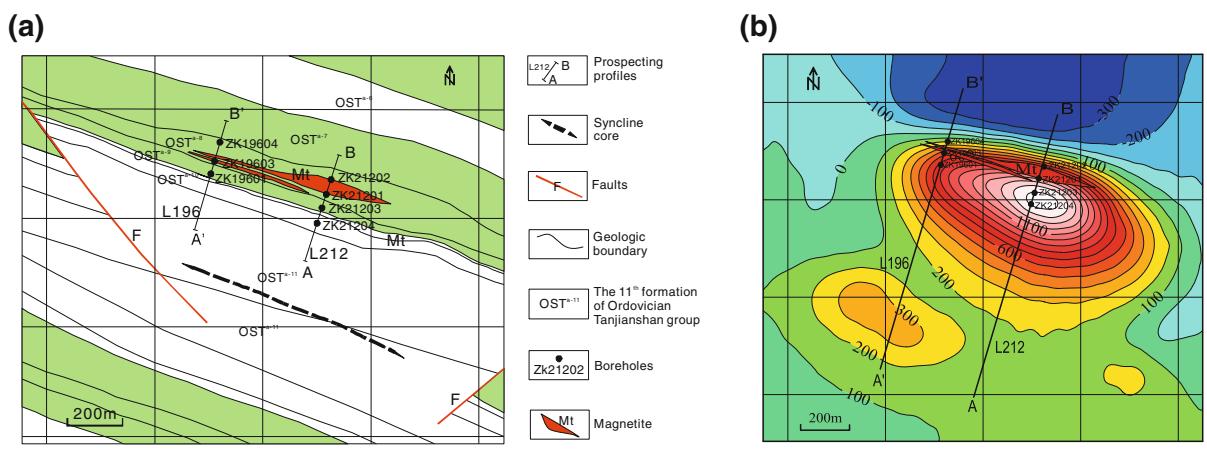

Figure 14
Geological map (**a**) and total field anomaly contour map (**b**) of the Galinge iron-ore deposit, Qinghai, northwestern China

Table 4

Statistics (geometric means) of magnetic properties of ore and rock samples of the Galinge iron-ore deposit, Qinghai, northwestern China

Ores and rocks	Number of samples	Susceptibility κ ($4\pi \times 10^{-6}$ SI)	Remanence J_r (10^{-3} A/m)	$Q = J_r/J_i$
Dense-massive magnetite	149	5.01×10^5	6.40×10^4	0.24
Dense-disseminated magnetite	280	1.39×10^5	2.12×10^4	0.28
Sparse-disseminated magnetite	171	4.23×10^4	2.86×10^4	1.26
Sparse-disseminated hema-magnetite	9	2.02×10^5	5.99×10^4	0.55
Mineralized marble	12	1.33×10^3	4.88×10^2	–
Skarnized marble	47	1.49×10^3	4.91×10^2	–
Grain-refining diorite	3	1.07×10^3	8.15×10^2	–
Mud siliceous	16	3.77×10^2	1.98×10^2	–
Magnet-mineralized diopsidite	16	1.52×10^4	3.02×10^4	–

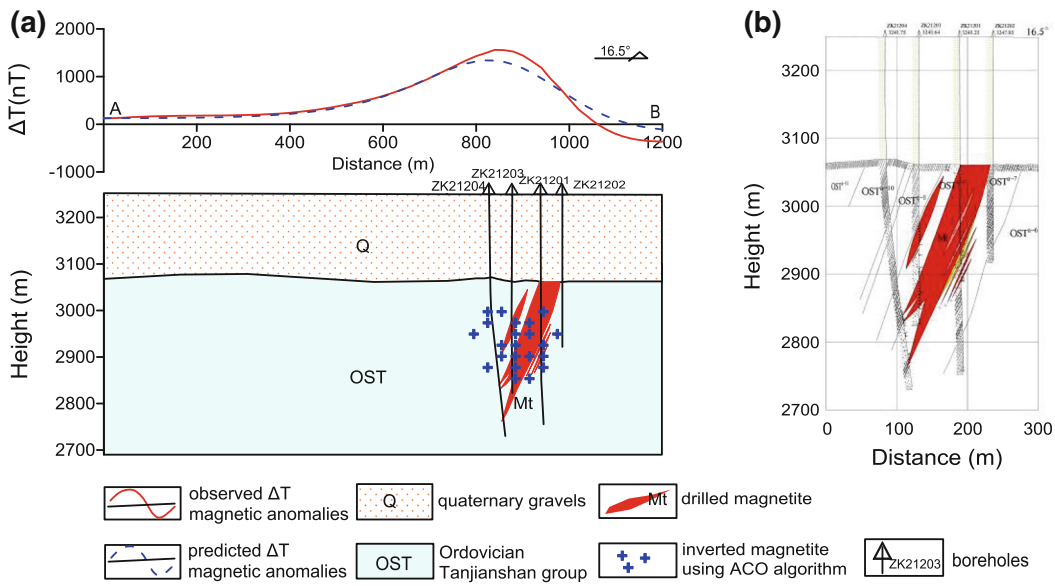

Figure 15

ACO binary representation imaging results for *line* 212 of the Galinge iron-ore deposit, Qinghai, northwestern China: **a** the inversion results and the observed and predicted magnetic anomalies, **b** the geological profile and drillholes. The inversion results are in good agreement with magnetite ores inferred from drillholes

The NP-ACO algorithm gives good results when prospecting for magnetite by use of ground magnetic anomalies.

5. *Prospecting for Granite by Use of Gravity Data in Nanling Region, Central China*

5.1. *Geology and Geophysics*

Nanling region is one of the most important mineralization belts of such endogenetic metals as tungsten, tin, copper, lead, and zinc in China. It is located in the structure-magmatic activities belt in the South China plate and goes though multi-phasic tectonic magmatism-mineralization. This area contains many types of granite and the mineralization is closely related to magmatic activity. It is, therefore, vitally important to study the distributions of granite. The density statistics show that in the Nanling area the average density of granite is 2.64 g/cm^3 whereas the average density of surrounding rocks of Paleozoic to Mesozoic strata is 2.69–2.73 g/cm^3. The residual

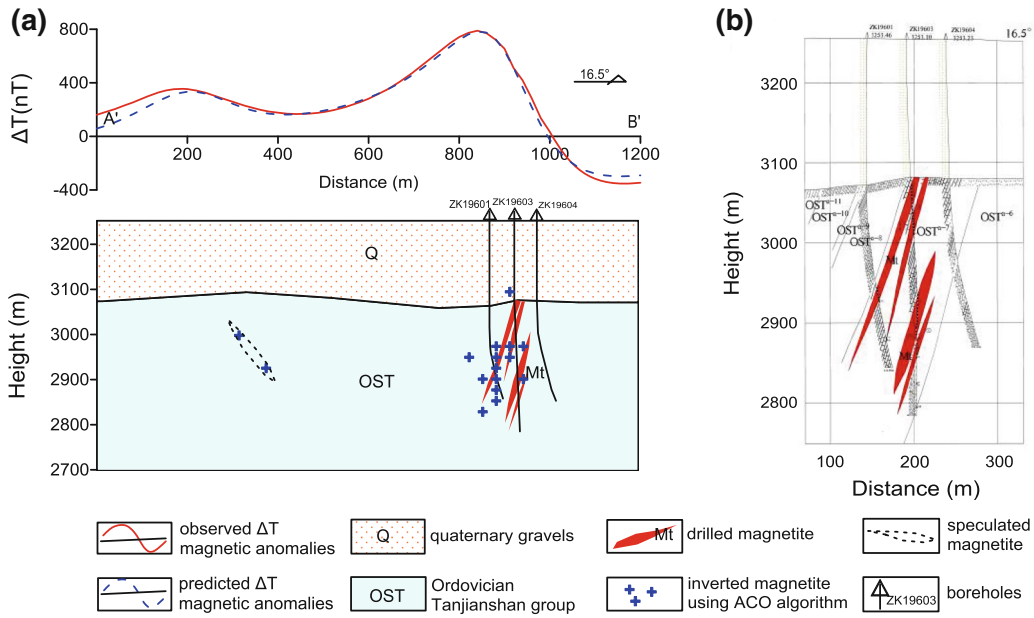

Figure 16

ACO binary representation imaging results of *line* 196 of the Galinge iron-ore deposit, Qinghai, northwestern China: **a** the inversion results and the observed and predicted magnetic anomalies, **b** the geological profile and drillholes. The inversion results are in good agreement with magnetite ores inferred from drillholes

Table 5

Statistics of density properties of rock samples in Nanling region, central China

Lithology	Density ρ (g/cm^3)		Lithology	Density ρ (g/cm^3)	
	Range	Geometric mean		Range	Geometric mean
Limestone	–	2.70	Syenite	–	2.65
Dolomite	2.73–2.75	2.74	Basement	–	2.84
Shale	–	2.53	Ultrabasic rock	–	2.91
Granite	2.55–2.63	2.60	Basalt	2.75–2.84	2.80
Granodiorite	2.62–2.67	2.64	Skarn	3.09–4.12	3.27

density of granite is -0.05 to -0.09 g/cm^3 (Table 5). Lower-density granites intruding into the sedimentary strata obviously cause negative gravity anomalies.

5.2. *Prospecting Jiuyi Mountain Granite by Use of NP-ACO*

Jiuyi Moutain rock in Nanling region is located in the well-known non-ferrous metal mining area. In this area fault structure and magmatic activity are common and ore-forming conditions are excellent (Fig. 17). We measured the gravity anomalies and the profile across the granite bodies. The Bouguer gravity anomalies reveal significant negative abnormal characteristics and the amplitude of negative anomalies reaches 24 mGal (Fig. 18). We used the binary representation imaging NP-ACO algorithm to invert the gravity anomalies to locate the distributions of granite.

When we used the NP-ACO to invert the 2D gravity anomalies and Jiuyi Mountain rock, the profile was divided into 40 columns $\times$ 20 rows $=$ 800 rectangular prisms. We assumed the number of ants was 200 and the pheromone volatility

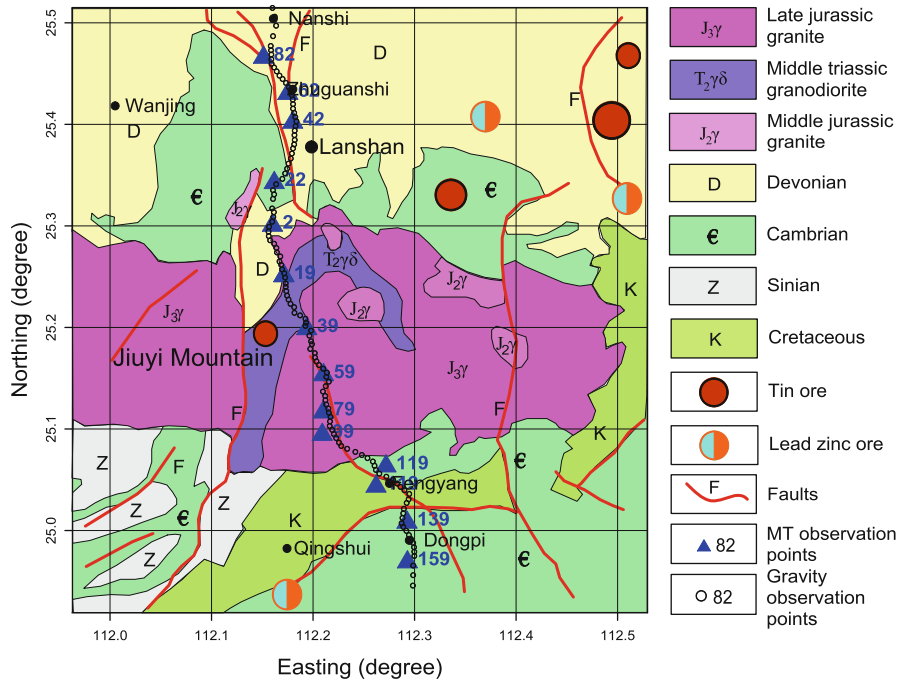

Figure 17
Diagram of Jiuyi Mountain rocks and the observation points of gravity and MT. The gravity and MT profiles cross the granite bodies

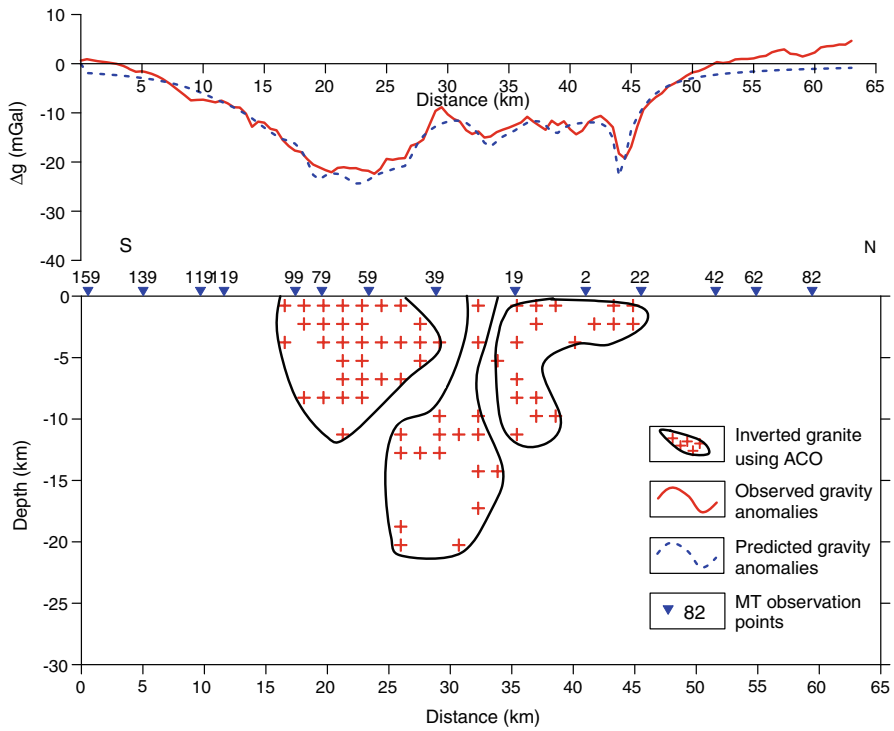

Figure 18
ACO binary representation imaging results for Jiuyi Mountain rocks of the Nanling region, central China. The inversion results reveal there are three main granite bodies in this profile

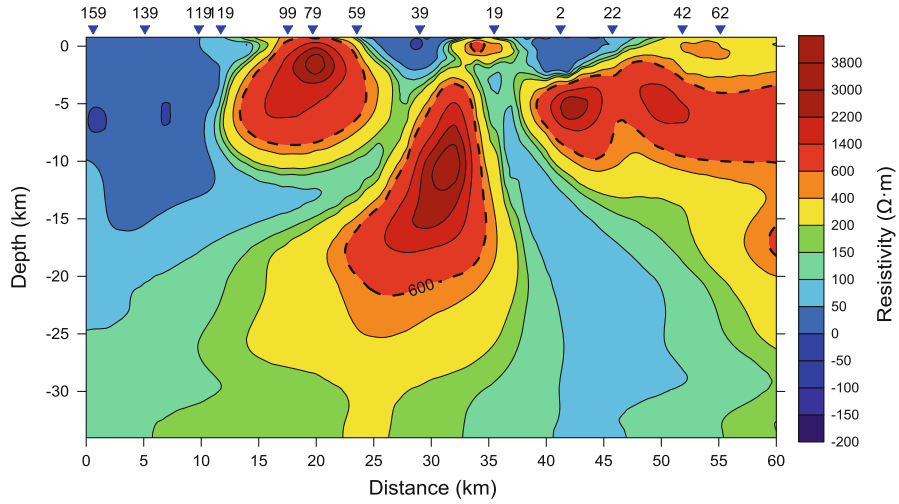

Figure 19
2D MT inversion results for Jiuyi Mountain rocks of the Nanling region, central China. The resistivity distributions indicate there are three main granite bodies in this profile

coefficient was 0.7. According to the density statistics results in this area (Table 5), the residual density of granite is -0.09 g/cm^3. The number of gravity observation points is 127, and the point spacing is 0.5 km. The ant colony converges after 31 iterations. The inversion results and garvity anomalies are shown in Fig. 18. This indicates that the predicted gravity anomalies accurately fit the observed gravity anomalies. Simultaneously, the inverted residual density distributions show that there are three granite rocks in this profile; some of the two southern granite rocks are outcroped whereas the northern granite rocks are concealed (Fig. 18). The outcroped locations of the granites are consistent with the surface geology (Fig. 17). With regard to depth, the middle granite rocks are deepest (22 km). The northern and shouthern rocks are shallower, with maxmium depths of approximately 10 km. The inversion results also coincide with the inversion results of the magnetotelluric (MT) method (Fig. 19). Resistivity distributions >600 Ω m are indicative of three high-resistivity bodies representing the three granite bodies. The maximum depth of the middle granite is 22 km. The depth of the southern granite is approximately 10 km and that of the northern concealed granite is also approximately 10 km. The depths of high resistivity distribution are in accordance with the NP-ACO inversion results. Overall, NP-ACO and MT reveal the depths and shapes of granite rocks accurately. This is helpful for study of the granite intrusion pattern and metallogenic regularity in the Nanling region.

6. *Conclusion*

Although the ACO algorithm is more widely used to solve the COP, it can also be used to invert potential field data by optimizing the objective function and dividing continuous model variables into discrete nodes. The ant colony tours the nodes to find the optimum solution, just as the salesman visits all the cities to search for the shortest routes in the TSP. This NP-ACO can be used for two types of potential field data inversion: parametric inversion of the simple shape model and imaging inversion of the complicated shape model. The method achieves good inversion results for both synthetic and real examples. Because it is based on the information positive feedback mechanism, the NP-ACO has better optimization capacity. It also has other intrinsic advantages, for example steady convergence, strong robustness, good parallel implementation, and convenient portability, compared with other stochastic metaheuristics. Both the binary representation imaging and full imaging ACO can produce sharper

physical property distributions than other linear inversion methods, for example PCG. The ACO has the potential to be a popular inversion approach for geophysical data inversion, similar to MC, GA, SA, ANN, etc. Nonetheless, because ground potential field data have lower resolution in the vertical direction, it is difficult to distinguish deeper or closed target bodies by use of this method. The NP-ACO also has some disadvantages. For instance, it takes too much time to find the shortest route and the ant colony is prone to mature too early, even though our proposed Gaussian mapping has greatly promoted the rate of convergence.

Acknowledgments

This work was supported by grants from the Natural Science Foundation of Hubei province (no. 2011CDA123), the Geological Survey Project of China (no. 12120113101800) and the National Basic Research Program of China (973 Program) (no. 2013CB733203). The authors thank the editor Dr Pierre Keating and the two anonymous reviewers for their constructive comments and suggestions, which significantly improved the manuscript. We also thank Dr Xiaoyang Wu, Dr Yuanyuan Li, and Dr Yushan Yang for their assistance.

References

Beckers, R., Deneubourg, J. L., and Goss, S. (1992), *Trails and U-turns in the selection of a path by the ant Lasius niger*, Journal of Theoretical Biology, *159*, 397–415.

Bullnheimer, B., Hartl, R. F., and Strauss, C. (1997), *Applying the ant system to the vehicle routing problem*, 2nd International Conference on Metaheuristics (MIC'97), 109–120.

Bullnheimer, B., Hartl, R. F., and Strauss, C. (1999), *An improved ant System algorithm for the vehicle Routing Problem*, Annals of Operations Research, *89*, 319-328.

Chen, S., Wang, S., and Zhang, Y. (2005a), *Ant colony optimization for the seismic nonlinear inversion*, 75th Annual International Meeting, SEG, Expanded Abstracts, 1732–1734.

Chen, S., Wang, S., Ji, M., and Zhang, Y. (2005b), *The ant colony algorithm for the seismic impedance inversion*, Geophysical Prospecting Petroleum, *44*, 551–553 (in Chinese with English abstract).

Coleman, C. M., Rothwell, E. J., and Ross, J. E. (2004), *Investigation of simulated annealing, ant-colony optimization, and genetic algorithms for self-structuring antennas*, IEEE Transactions on Antennas and Propagation, *52*, 1007–1014.

Colorni, A., Dorigo, M., and Maniezzo, V. (1991), *Distributed optimization by ant colonies*, Proceedings of the 1st European Conference on Artifical Life, 134–142.

Colorni, A., Dorigo, M., Maniezzo, V., and Trubian, M. (1994), *Ant system for job-shop scheduling*, Belgian Journal of Operations Research, Statistics and Computer Science, *34*, 39–53.

Colton, D., Piana, M., and Potthast, R. (1997), *A simple method using Morozov's discrepancy principle for solving inverse scattering problems*, Inverse Problems, *13*, 1477.

Di Caro, G., and Dorigo, M. (1998a), *AntNet: Distributed stigmergetic control for communications networks*, Journal of Articial Inteligence Research, *9*, 317–365.

Di Caro, G., and Dorigo, M. (1998b), *Two ant colony algorithms for best-effort routing in datagram networks*, Proceedings of the 10th IASTED International Conference on Parallel and Distributed Computing and Systems (PDCS'98), 541–546.

Dorigo, M. (1992), *Optimization, learning and natural algorithms*, Ph. D. Thesis, Politecnico di Milano.

Dorigo, M., and Gambardella, L. M. (1997a), *Ant colony system: A cooperative learning approach to the traveling salesman problem*, IEEE Transactions on Evolutionary Computation, *1*, 53–66.

Dorigo, M., and Gambardella, L. M. (1997b), *Ant colonies for the travelling salesman problem*, BioSystems, *43*, 73–82.

Dorigo, M., and Stutzle, T. (2003), *The ant colony optimization metaheuristic: Algorithms, applications, and advances, in F. Glover and G. Kochenberger, eds., Handbook of metaheuristics*, Kluwer Academic Publishers, 250–285.

Dorigo, M., and Blum, C. (2005), *Ant colony optimization theory: A survey*, Theoretical computer science, *344*, 243–278.

Dorigo, M., Maniezzo, V., and Colorni, A. (1991), *The ant system: An autocatalytic optimizing process*, Politecnico di Milano, 91–016.

Dorigo, M., Maniezzo, V., and Colorni, A. (1996), *Ant system: optimization by a colony of cooperating agents*, IEEE Trans on Systems, Man, and Cybernetics- Part B: Cybernetics, *26*, 29–41.

Dorigo, M., Di Caro, G., and Gambardella, L. M. (1999), *Ant algorithms for discrete optimization*, Artificial life, *5*, 137–172.

Gambardella, L., Taillard, E., and Dorigo, M. (1997), *Ant colonies for the QAP*, Istituto Dalle Molle di Studi sull'Intelligenza Artificiale (IDSIA), 4–97.

Gambardella, L. M., and Dorigo, M. (1995), *Ant-Q: A reinforcement learning approach to the traveling salesman problem*, Proceedings of the 12th International Conferences on Machine Learning (ML'95), Palo Alto, CA: Morgan Kauffman, 252–260.

Gambardella, L. M., and Dorigo, M. (1996), *Solving symmetric and asymmetric TSPs by ant colonies*, Proceedings of the 3rd IEEE International Conference on Evolutionary Computation, Nagoya, 622–627.

Gambardella, L. M., Taillard, E., and Agazzi, G. (1999a), *Macs-vrptw: A multiple colony system for vehicle routing problems with time windows, in D. Corne, M. Dorigo and F. Glover eds., New ideas in optimization*, Istituto Dalle Molle Di Studi Sull Intelligenza Artificiale (IDSIA), Maidenhead, UK: McGraw-Hill., 63–76.

Gambardella, L. M., Taillard, E., and Dorigo, M. (1999b), *Ant colonies for the quadratic assignment problem*, Journal of the Operational Research Society, *50*, 167–176.

Golub, G. H., and Von matt, U. (1997), *Generalized cross-validation for large-scale problems*, Journal of Computational and Graphical Statistics, *6*, 1–34.

GOLUB, G. H., HEATH, M., and WAHBA, G. (1979), *Generalized cross-validation as a method for choosing a good ridge parameter*, Technometrics, *21*, 215–223.

GOSS, S., ARON, S., DENEUBOURG, J. L., and PASTEELS, J. M. (1989), *Self-organized shortcuts in the Argentine ant*, Naturwissenschaften, *76*, 579–581.

LEE, Z., SU, S., CHUANG, C., and LIU, K. (2008), *Genetic algorithm with ant colony optimization (GA-ACO) for multiple sequence alignment*, Applied Soft Computing, *8*, 55–78.

LELIEVRE, P. G., and OLDENBURG, D. W. (2009), *A 3D total magnetization inversion applicable when significant, complicated remanence is present*, Geophysics, *74*, L21–L30.

LI, Y., and OLDENBURG, D. W. (1996), *3-D inversion of magnetic data*, Geophysics, *61*, 394–408.

LI, Y., and OLDENBURG, D. W. (1998), *3-D inversion of gravity data*, Geophysics, *63*, 109–119.

LI, Y., and OLDENBURG, D. W. (2000), *Joint inversion of surface and three-component borehole magnetic data*, Geophysics, *65*, 540–552.

LIU, T. (2007), *New data processing methods for potential field exploration*, Science Press, Beijing, 103–106 pp.

MANIEZZO, V. (1999), *Exact and approximate nondeterministic tree-search procedures for the quadratic assignment problem*, INFORMS Journal on Computing, *11*, 358–369.

MANIEZZO, V., and COLORNI, A. (1999), *The ant system applied to the quadratic assignment problem*, IEEE Transactions on Knowledge and Data Engineering, *11*, 769–778.

PILAT, M., and WHITE, T. (2002), *Using genetic algorithms to optimize ACS-TSP*, Proceedings of the 3rd International Workshop on Ant Algorithms (ANTS'02), 101–172.

PILKINGTON, M. (1997), *3-D magnetic imaging using conjugate gradients*, Geophysics, *62*, 1132–1142.

QI, J., YE, J., and BAO, S. (2010), *Analysis of the geological features and genesis of the ga linge railmult-imetal deposits*, Journal Qinghai University (natural science edition), *28*, 42–46 (in Chinese with English abstract).

SCHERZER, O. (1993), *The use of Morozov's discrepancy principle for Tikhonov regularization for solving nonlinear ill-posed problems*, Computing, *51*, 45–60.

SCHOONDERWOERD, R., HOLLAND, O. E., BRUTEN, J. L., and ROTHKRANTZ, L. J. M. (1997), *Ant-based load balancing in telecommunications networks*, Adaptive Behavior, *5*, 169–207.

SIVAGAMINATHAN, R. K., and RAMAKRISHNAN, S. (2007), *A hybrid approach for feature subset selection using neural networks and ant colony optimization*, Expert Systems with Applications, *33*, 49–60.

SOCHA, K., and BLUM, C. (2007), *An ant colony optimization algorithm for continuous optimization: application to feed-forward neural network training*, Neural Computing & Applications, *16*, 235–247.

SOCHA, K., and DORIGO, M. (2008), *Ant colony optimization for continuous domains*, European Journal of Operational Research, *185*, 1155–1173.

STUTZLE, T., and HOOS, H. (1997a), *MAX-MIN Ant System and local search for combinatorial optimization problems, in V. Stefan, M. Silvano, H. O. Ibrahim and R. Catherine eds., Meta-Heuristics: Advances and Trends in Local Search Paradigms for Optimization*, Kluwer Academic Publishers, 137–154.

STUTZLE, T., and HOOS, H. (1997b), *MAX-MIN ant system and local search for the traveling salesman problem*, Proceedings of IEEE International Conference on Evolutionary Computation and Evolutionary Programming Conference (IEEE-ICEC-EPS'97), Piscataway, 309–314.

STUTZLE, T., and HOOS, H. (1998), *Improvements on the Ant System: MAX-MIN Ant System*, Proceedings of Artificial Neural Nets and Genetic Algorithms, Springer-Verlag, 245–249.

STUTZLE, T., and DORIGO, M. (2002), *A short convergence proof for a class of ant colony optimization algorithms*, IEEE Trans. Evolutionary Computation, *6*, 358–365.

TIKHONOV, A., and ARSENIN, V. Y. (1977), *Solutions of ill-posed problems*, V. H. Winston & Sons, Washington, D.C., 87–94 pp.

YAN, Z., GU, H., and ZHAO, X. (2009), *Non-linear AVO inversion based on ant colony algorithm*, Oil Geophysical Prospecting, *44*, 700–702 (in Chinese with English abstract).

YUAN, S., WANG, S., and TIAN, N. (2009), *Swarm intelligence optimization and its application in geophysical data inversion*, Applied Geophysics, *6*, 166–174.

ZHANG, H., LIU, T., ZHU, C., and ZHOU, Z. (2011), *The effects of applying high-precision magnetic survey: a case study of the Galinge ore district in Qinghai province*, Geophysical and Geochemical Exploration, *35*, 12–16 (in Chinese with English abstract).

ZHANG, S. (2003), *Process method study of oceanic satellite altimetry gravity data and its application in Okinawa Trough*, Ph. D. Thesis, China University of Geosciences.

(Received March 29, 2013, revised August 12, 2013, accepted August 20, 2013, Published online October 5, 2013)